Inorg. Chem. **2005**, *44*, 9023–9038

Electrochemistry and Spectroelectrochemistry of Heterobimetallic Porphyrin–Corrole Dyads. Influence of the Spacer, Metal Ion, and Oxidation State on the Pyridine Binding Ability

Karl M. Kadish,*,† Jianguo Shao,†,§ Zhongping Ou,† Riqiang Zhan,† Fabien Burdet,‡ Jean-Michel Barbe,‡ Claude P. Gros,‡ and Roger Guilard*,‡

Department of Chemistry, University of Houston, Houston, Texas 77204-5003, and LIMSAG UMR 5633, Faculté des Sciences Gabriel, Université de Bourgogne, 6 boulevard Gabriel, 21000 Dijon, France

Received June 29, 2005

Combined electrochemical and UV–visible spectroelectrochemical methods were utilized to elucidate the prevailing mechanisms for electroreduction of previously synthesized porphyrin–corrole dyads of the form (PCY)H_2Co and (PCY)MClCoCl where M = Fe^{III} or Mn^{III}, PC = porphyrin–corrole, and Y is a bridging group, either biphenylenyl (B), 9,9-dimethylxanthenyl (X), anthracenyl (A), or dibenzofuranyl (O). These studies were carried out in pyridine, conditions under which the cobalt(IV) corrole in (PCY)MClCoCl is immediately reduced to its Co^{III} form, thus enabling direct comparisons with the free-base porphyrin dyad, (PCY)H_2Co^{III} under the same solution conditions. The compounds are all reduced in multiple one-electron-transfer steps, the first of which involves the M^{III}/M^{II} process of the porphyrin in the case of (PCY)MClCoCl and the Co^{III}/Co^{II} process of the corrole in the case of (PCY)H_2Co. Each metal-centered redox reaction may be accompanied by the gain or loss of pyridine axial ligands, with the exact stoichiometry of the exchange process depending upon the specific combination of metal ions in the dyad, their oxidation states, and the particular spacer in the complex. Before this study was started, it was expected that the porphyrin–corrole dyads with the largest spacers, namely, O and A, would readily accommodate the formation of cobalt(III) bis-pyridine adducts because of the larger size of the cavity while dyads with the smallest B spacer would seem to have insufficient room to add even a single pyridine within the cavity, as was structurally seen in the case of (PCB)H_2Co(py). This is clearly not the case, as shown in the present study. A reversible Co^{III}/Co^{II} reaction is seen for (PCB)MnClCoCl at –0.62 V, which when combined with spectroscopic data, leads to the assignment of (PCB)$Mn^{III}(py)_2Co^{III}$(py) as the species in pyridine. The reduction of (PCB)$Mn^{III}(py)_2Co^{III}$(py) to (PCB)Mn^{II}(py)Co^{III}(py) is accompanied on the slower spectroelectrochemical time scale by the appearance of a 603 nm band in the UV–vis spectra and is consistent with the addition of a second pyridine ligand to the Co^{III}(py) unit of the dyad as one ligand is lost from the electrogenerated manganese(II) porphyrin, thus maintaining one pyridine ligand within the cavity. A different change in the coordination number is observed in the case of (PCB)FeClCoCl. Here the initial Fe^{III} complex can be assigned as (PCB)$Fe^{III}Cl Co^{III}$(py), which has no pyridine molecule within the cavity and the singly reduced form is characterized as (PCB)$Fe^{II}(py)_2Co^{III}(py)_2$, which contains two pyridine ligands inside the cavity. A following one-electron reduction of the Fe^{II}/Co^{III} complex then gives $[(PCB)Fe^{II}(py)_2Co^{II}]^-$.

Introduction

The synthesis and reactivity of numerous face-to-face-linked bis-porphyrins[1−10] and bis-phthalocycanines[11] have been reported in the literature. Many of these dyads contain free-base macrocycles or macrocycles with electroinactive metal ions such as Zn^{II}, while others contain one or more

* To whom correspondence should be addressed. E-mail: KKadish@uh.edu (K.K.), Roger.Guilard@u-bourgogne.fr (R.G.).
† University of Houston.
‡ Université de Bourgogne.
§ Current address: Department of Chemistry, Midwestern State University, 3410 Taft Blvd., Wichita Falls, TX 76308-2099.

(1) (a) Le Mest, Y.; L'Her, M.; Hendricks, N. H.; Kim, K.; Collman, J. P. *Inorg. Chem.* **1992**, *31*, 835−847. (b) Le Mest, Y.; L'Her, M.; Saillard, J.-Y. *Inorg. Chim. Acta* **1996**, *248*, 181−191. (c) Le Mest, Y.; L'Her, M.; Courtot-Coupez, J.; Collman, J. P.; Evitt, E. R.; Bencosme, C. S. *J. Electroanal. Chem.* **1985**, *184*, 331−346. (d) Le Mest, Y.; L'Her, M.; Collman, J. P.; Kim, K.; Hendricks, N. H.; Helm, S. *J. Electroanal. Chem.* **1987**, *234*, 277−295.

10.1021/ic051073s CCC: $30.25
Published on Web 10/26/2005

redox-active ions, with examples being complexes with iron, manganese, ruthenium, or cobalt centers where M^{III}/M^{II} processes are readily observed.

Our own interest in face-to-face bis-macrocycles has focused in large part on the electrochemistry, ligand binding reactions, and spectroscopic properties of bis-corrole and porphyrin−corrole dyads containing redox-active metal centers.[12] These have included bis-copper,[13] bis-nickel,[14] and bis-cobalt[15,16] derivatives, the latter of which were shown to be effective catalysts in the four-electron reduction of O_2 when adsorbed on a graphite electrode in acid media.[17] The synthesis and characterization of free-base porphyrins linked to a cobalt(III) corrole[18] and heterobimetallic dyads containing iron(III) or manganese(III) porphyrins linked in a face-to-face arrangement with a cobalt(IV) corrole have also been reported by our group.[19] Each heterobinuclear complex was

Chart 1. Structures of Investigated Compounds

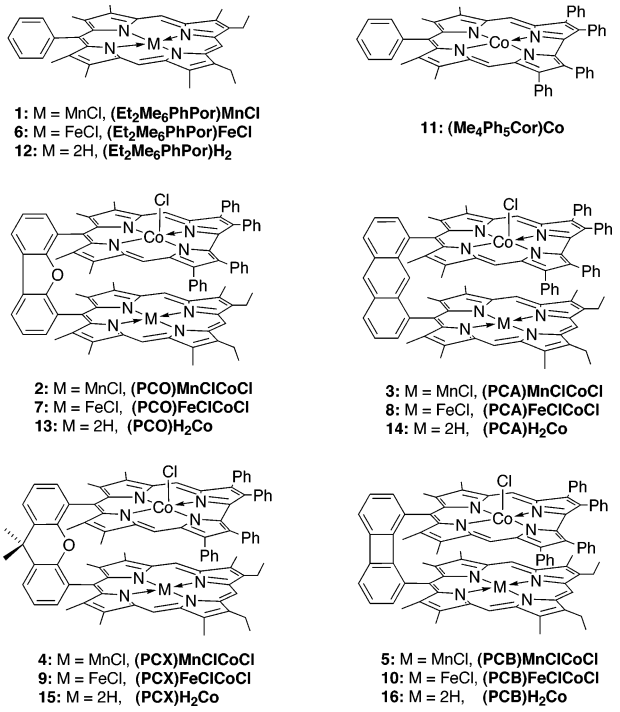

characterized by mass spectrometry, UV−visible, IR, and electron spin resonance spectroscopies as well as by electrochemistry in nonbonding or weakly bonding media. These dyads are represented as $(PCY)H_2Co^{III}$ and $(PCY)MClCo^{IV}Cl$ where PC = porphyrin−corrole, M = Mn^{III} or Fe^{III}, and Y is a bridging group, either biphenylenyl (B), 9,9-dimethylxanthenyl (X), anthracenyl (A), or dibenzofuranyl (O) (see Chart 1).

Manganese porphyrins,[20] iron porphyrins,[20] and cobalt corroles[12,21,22] can each exist in a variety of metal oxidation states, and this is investigated in the present paper, which examines the electrochemistry and spectroelectrochemistry of the above $(PCY)MClCo^{IV}Cl$ and related $(PCY)H_2Co^{III}$ dyads (Chart 1) in pyridine, a solvent known to coordinate to both the porphyrin and corrole metal centers, thus giving complexes with one to four axially bound ligands depending upon the type of metal ion in the porphyrin, the metal oxidation state in both macrocycles, and the type of spacer linking the two macrocycles.

The binding of small molecules, nitrogenous bases, and other axial ligands to one or both metal ions in the face-to-face bis-porphyrin has been well-documented in the litera-

(2) (a) Rosenthal, J.; Pistorio, B. J.; Chng, L. L.; Nocera, D. G. *J. Org. Chem.* **2005**, *70*, 1885−1888. (b) Chng, L. L.; Chang, C. J.; Nocera, D. G. *J. Org. Chem.* **2003**, *68*, 4075−4078. (c) Chang, C. J.; Baker, E. A.; Pistorio, B. J.; Deng, Y.; Loh,; Miller, S. E.; Carpenter, S. D.; Nocera, D. G. *Inorg. Chem.* **2002**, *41*, 3102−3109. (d) Deng, Y.; Chang, C. J.; Nocera, D. G. *J. Am. Chem. Soc.* **2000**, *122*, 410−411. (e) Chang, C, J.; Deng, Y.; Heyduk, A. F.; Chang, C. K.; Nocera, D. G. *Inorg. Chem.* **2000**, *39*, 959−966.

(3) Osuka, A.; Nakajima, S.; Maruyama, K.; Mataga, N.; Asahi, T.; Yamazaki, I.; Nishimura, Y.; Ohno, T.; Nozaki, K. *J. Am. Chem. Soc.* **1993**, *115*, 4577−4589.

(4) (a) Funatsu, K.; Imamura, T.; Ichimura, A.; Sasaki, Y. *Inorg. Chem.* **1998**, *37*, 4986−4995. (b) Fukushima, K.; Funatsu, K.; Ichimura, A.; Sasaki, Y.; Suzuki, M.; Fujihara, T.; Tsuge, K.; Imamura, T. *Inorg. Chem.* **2003**, *42*, 3187−3193. (c) Imamura, T.; Funatsu, K.; Ye, S.; Morioka, Y.; Uosaki, K.; Sasaki, Y. *J. Am. Chem. Soc.* **2000**, *122*, 9032−9033.

(5) (a) Fletcher, J. T.; Therien, M. J. *J. Am. Chem. Soc.* **2002**, *124*, 4298−4311. (b) Fletcher, J. T.; Therien, M. J. *Inorg. Chem.* **2002**, *41*, 331−341.

(6) (a) Fukuzumi, S.; Okamoto, K.; Tokuda, Y.; Gros, C. P.; Guilard, R. *J. Am. Chem. Soc.* **2004**, *126*, 17059−17066. (b) Fukuzumi, S.; Okamoto, K.; Gros, C. P.; Guilard, R. *J. Am. Chem. Soc.* **2004**, *126*, 10441−10449.

(7) Brettar, J.; Gisselbrecht, J.-P.; Gross, M.; Solladié, N. *Chem. Commun.* **2001**, 733−734.

(8) Wylie, R. S.; Levy, E. G.; Sanders, J. K. M. *Chem. Commun*. **1997**, 1611−1612.

(9) Yagi, S.; Yonekura, I.; Awakura, M.; Ezoe, M.; Takagishi, T. *Chem. Commun*. **2001**, 557−558.

(10) Tomohiro, Y.; Satake, A.; Kobuke, Y. *J. Org. Chem.* **2001**, *66*, 8442−8446.

(11) (a) Nikolaitchik, A. V.; Rodgers, M. A. J. *J. Phys. Chem. A* **1999**, *103*, 7597−7605. (b) Nikolaitchik, A. V.; Korth, O.; Rodgers, M. A. J. *J. Phys. Chem. A* **1999**, *103*, 7587−7596.

(12) Guilard, R.; Barbe, J.-M.; Stern, C.; Kadish, K. M. In *The Porphyrin Handbook*; Kadish, K. M., Smith, K. M., Guilard, R., Eds.; Elsevier: New York, 2003; Vol. 18, pp 303−349.

(13) Guilard, R.; Gros, C. P.; Barbe, J.-M.; Espinosa, E.; Jérôme, F.; Tabard, A.; Latour, J.-M.; Shao, J.; Ou, Z.; Kadish, K. M. *Inorg. Chem*. **2004**, *43*, 7441−7455.

(14) Jérôme, F.; Barbe, J.-M.; Gros, C. P.; Guilard, R.; Fischer, J.; Weiss, R. *New J. Chem*. **2001**, *25*, 93−101.

(15) Guilard, R.; Jérôme, F.; Barbe, J.-M.; Gros, C. P.; Ou, Z.; Shao, J.; Fischer, J.; Weiss, R.; Kadish, K. M. *Inorg. Chem.* **2001**, *40*, 4856−4865.

(16) Kadish, K. M.; Ou, Z.; Shao, J.; Gros, C. P.; Barbe, J.-M.; Jérôme, F.; Bolze, F.; Burdet, F.; Guilard, R. *Inorg. Chem.* **2002**, *41*, 3990−4005.

(17) Kadish, K. M.; Frémond, L.; Ou, Z.; Shao, J.; Shi, C.; Anson, F. C.; Burdet, F.; Gros, C. P.; Barbe, J.-M.; Guilard, R. *J. Am. Chem. Soc.* **2005**, *127*, 5625−5631.

(18) Kadish, K. M.; Shao, J.; Ou, Z.; Frémond, L.; Zhan, R.; Burdet, F.; Barbe, J.-M.; Gros, C. P.; Guilard, R. *Inorg. Chem*. **2005**, *44*, 6744−6754.

(19) Guilard, R.; Burdet, F.; Barbe, J.-M.; Gros, C. P.; Espinosa, E.; Shao, J.; Ou, Z.; Zhan, R.; Kadish, K. M. *Inorg. Chem.* **2005**, *44*, 3972−3983.

(20) (a) Kadish, K. M.; Van Caemelbecke, E.; Royal, G. In *The Porphyrin Handbook*; Kadish, K. M., Smith, K. M., Guilard, R., Eds.; Academic Press: San Diego, CA, 2000; Vol. 8, pp 1−97. (b) Kadish, K. M.; Royal, G.; Van Caemelbecke, E.; Gueletti, L. In *The Porphyrin Handbook*; Kadish, K. M., Smith, K. M., Guilard, R., Eds.; Academic Press: San Diego, CA, 2000; Vol. 9, pp 1−220. (c) Weiss, R.; Gold, A.; Trautwein, A. X.; Terner, J. In *The Porphyrin Handbook*; Kadish, K. M., Smith, K. M., Guilard, R., Eds.; Academic Press: San Diego, CA, 2000; Vol. 4, pp 65−96.

(21) Erben, C.; Will, S.; Kadish, K. M. In *The Porphyrin Handbook*; Kadish, K. M., Smith, K. M., Guilard, R., Eds.; Academic Press: San Diego, CA, 2000; Vol. 2, pp 233−300.

(22) Paolesse, R. In *The Porphyrin Handbook*; Kadish, K. M., Smith, K. M., Guilard, R., Eds.; Academic Press: San Diego, CA, 2000; Vol. 2, pp 201−232.

Scheme 1. Schematic Representation of Metal-Centered (PCY)$M^{III}ClCo^{IV}Cl$ Redox Reactions

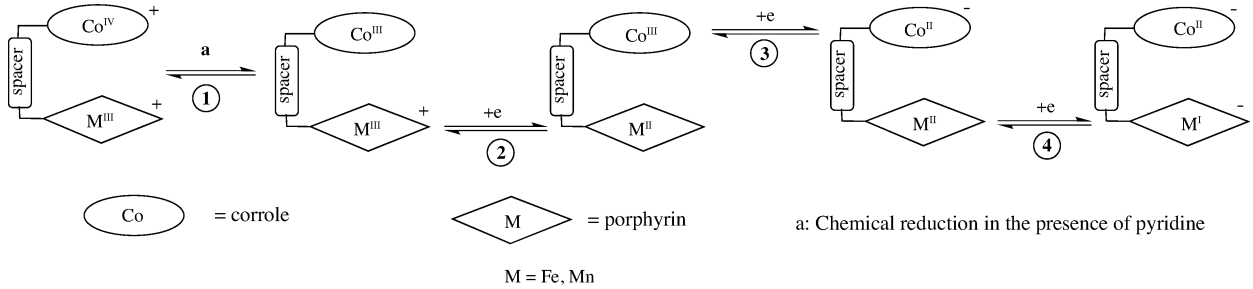

ture,[7,8,23] and an understanding of these processes is essential in designing cofacial bis-macrocyclic systems that possess an optimum separation between the two metal centers in order to obtain a desired cooperativity between the two macrocyclic units for the purpose of carrying out a specific chemical or photochemical reaction.[24] In this regard, it is necessary to evaluate the ligand binding properties of the dyad in a variety of oxidation states because changes in the metal oxidation state are often associated with a specific chemical or photochemical reaction being carried out by the dyad. It is also necessary to determine how the cooperativity between the two face-to-face macrocycles will change upon varying the cavity size within the dyad, and this was accomplished in our laboratory[15−17] and others[1,2,25] by changing the type of bridge that links the two macrocycles. However, despite many advances in this area, there are very little data in the literature demonstrating how axial coordination of a face-to-face bis-macrocycle will change upon systematically oxidizing or reducing the central metal ion.

This is investigated in the present paper, which reports how the redox reactivity and pyridine binding ability of each individual macrocycle of the investigated dyads will mutually influence each other upon going from a high to a low metal oxidation state of the porphyrin and/or the corrole in the face-to-face configuration. This is accomplished by examining the prevailing electrochemistry of the dyads using cyclic voltammetry and thin-layer spectroelectrochemistry and then comparing the data to those of the related mono-porphyrin and -corrole under the same solution conditions. An elucidation of ligand binding equilibria is relatively simple in the case of $(PCY)H_2Co$ because the cobalt(III) but not cobalt(II) corrole will bind pyridine, and the coordination number of Co^{III} in pyridine can be unambiguously assigned on the basis of spectroscopic and electrochemical data. A more complex behavior, however, is observed in the case of (PCY)MClCoCl ($M = Fe^{III}$, Mn^{III}) where multiple metal oxidation states of the dyad can be electrogenerated,[19] each of which will have a different pyridine binding ability. Under these conditions, one must consider iron(III), -(II), and -(I) porphyrins linked to cobalt(IV), -(III), or -(II) corroles in the case of $(PCY)Fe^{III}ClCo^{IV}Cl$ and manganese(III) or -(II) porphyrins linked to cobalt(IV), -(III), or -(II) corroles in the case of $(PCY)Mn^{III}ClCo^{IV}Cl$.

The stepwise conversion of iron(III) or manganese(III) porphyrins to their lower oxidation states is shown in Scheme 1, which illustrates the oxidation states of the two metal ions but not the degree of axial coordination. As will be demonstated, $(PCY)M^{III}ClCo^{IV}Cl$ is rapidly reduced to its M^{III}/Co^{III} form upon dissolution in pyridine (reaction 1), after which the metal-centered electroreductions of the dyad occur in a stepwise fashion upon application of an appropriate potential, first at the Mn^{III} or Fe^{III} ion of the porphyrin (reaction 2), then by reduction of the cobalt(III) corrole to its Co^{II} form (reaction 3), and then, at more negative potentials, by reduction of the porphyrin, giving an iron(I) complex in the case of (PCY)FeClCoCl (reaction 4) or a manganese(II) porphyrin π-anion radical in the case of (PCY)MnClCoCl (not shown in Scheme 1). Additional reductions of the cobalt(II) corrole and manganese(II) or iron(II) porphyrins to their π-anion radical forms also occur, but these processes were not examined in the present paper, which concentrates on those redox reactions that involve changes in the metal ion oxidation state and changes in axial coordination.

As will be shown, a characterization of $(PCY)H_2Co$ electrochemistry and pyridine binding is relatively straightforward, and this contrasts with the case of (PCY)MClCoCl in pyridine (py) where the iron(III) or manganese(III) porphyrin (Por) can exist with four different sets of axial ligands, with examples being $(Por)M^{III}Cl$, $(Por)M^{III}Cl(py)$, $[(Por)M^{III}(py)]^+$, or $[(Por)M^{III}(py)_2]^+$ for M^{III} ions and $(Por)M^{II}(py)$ or $(Por)M^{II}(py)_2$ for the electrogenerated metal-(II) porphyrins, each of which may interact to a different extent with the linked cobalt corrole depending upon the size

(23) (a) Sanders, J. K. M. In *The Porphyrin Handbook*; Kadish, K. M., Smith, K. M., Guilard, R., Eds.; Academic Press: San Diego, CA, 2000; Vol. 3, pp 347−368. (b) Tabushi, I.; Kugimiya, S.-I.; Kinnaird, M. G.; Sasaki, T. *J. Am. Chem. Soc*. **1985**, *107*, 4192−4199. (c) Collman, J. P.; Hutchison, J. E.; Wagenknecht, P. S.; Lewis, N. S.; Lopez, M. A.; Guilard, R. *J. Am. Chem. Soc*. **1990**, *112*, 8206−8208. (d) Le Mest, Y.; L'Her, M.; Collman, J. P.; Hendricks, N. H.; McElwee-White, L. *J. Am. Chem. Soc.* **1986**, *108*, 533−535. (e) Ward, B.; Wang, C.-B.; Chang, C. K. *J. Am. Chem. Soc.* **1981**, *103*, 5236−5238. (f) Chang, C. K. *J. Chem. Soc., Chem. Commun*. **1977**, 800−801.

(24) (a) Harvey, P. D. In *The Porphyrin Handbook*; Kadish, K. M., Smith, K. M., Guilard, R., Eds.; Elsevier: San Diego, 2003; Vol. 18, pp 63−250. (b) Bolze, F.; Gros, C. P.; Drouin, M.; Espinosa, E.; Harvey, P. D.; Guilard, R. *J. Organomet. Chem.* **2002**, 89−97. (c) Faure, S.; Stern, C.; Espinosa, E.; Douville, J.; Guilard, R.; Harvey, P. D. *Chem., Eur. J.* **2005**, *11*, 3469−3481. (d) Chang, C. J.; Loh, Z.-H.; Deng, Y.; Nocera, D. G. *Inorg. Chem.* **2003**, *42*, 8262−8269. (e) Faure, S.; Stern, C.; Guilard, R.; Harvey, P. D. *J. Am. Chem. Soc.* **2004**, *126*, 1253−1261. (f) Hodgkiss, J. M.; Chang, C. J.; Pistorio, B. J.; Nocera, D. G. *Inorg. Chem.* **2003**, *42*, 8270−8277. (g) Fukuzumi, S.; Ohkubo, K.; E. W.; Ou, Z.; Shao, J.; Kadish, K. M.; Hutchison, J. A.; Ghiggino, K. P.; Sintic, P. J.; Crossley, M. J. *J. Am. Chem. Soc.* **2003**, *125*, 14984−14985.

(25) (a) Collman, J. P.; Boulatov, R.; Sunderland, C. J. In *The Porphyrin Handbook*; Kadish, K. M., Smith, K. M., Guilard, R., Eds.; Elsevier: San Diego 2003; Vol. 62, pp 1−49. (b) Collman, J. P.; Wagenknecht, P. S.; Hutchison, J. E. *Angew. Chem., Int. Ed. Engl.* **1994**, *33*, 1537−1554.

Table 1. UV−Visible Spectral Data [λ_{max}, nm ($\epsilon \times 10^{-4}$, L mol^{-1} cm^{-1})] of Neutral and Electroreduced Manganese Porphyrin−Corrole[a] Dyads in Pyridine Containing 0.1 M TBAP

		Soret region				Q region	
metal ions	macrocycle						$Co^{III}(py)_2$
Co^{III}	Me_4Ph_5Cor (**11**)			433 (3.5)		557 (0.7)	598 (1.7)
Mn^{III}	Et_2Me_6PhPor (**1**)	375 (7.9)	396 (sh, 3.8)		474 (4.8)	553 (1.0)	
Mn^{III}/Co^{III}	PCO (**2**)	377 (8.2)	399 (sh, 6.3)	415 (sh, 6.0)	474 (3.8)	554 (0.9)	598 (1.7)
	PCA (**3**)	376 (6.1)	401 (sh, 4.6)	421 (sh, 4.4)	475 (3.1)	556 (0.6)	600 (1.7)
	PCX (**4**)	373 (6.7)	407 (sh, 3.6)	423 (sh, 3.3)	475 (2.2)	554 (0.8)	599 (0.9)
	PCB (**5**)	368 (9.6)		420 (sh, 2.5)	478 (1.0)	554 (0.7)	none
Mn^{II}	Et_2Me_6PhPor (**1**)	352 (3.3)		430 (16.6)		555 (1.4)	
Mn^{II}/Co^{III}	PCO (**2**)	355 (3.9)		430 (13.7)		555 (1.6)	598 (1.7)
	PCA (**3**)	355 (2.8)		431 (11.4)		557 (0.9)	600 (1.7)
	PCX (**4**)	355 (3.4)		429 (11.2)		556 (1.2)	600 (1.4)
	PCB (**5**)	379 (6.8)	413 (7.1)	432 (sh, 6.7)		560 (1.0)	603 (0.8)

[a] Mn^{III} and Mn^{III}/Co^{III} represent the neutral compounds, while Mn^{II} and Mn^{II}/Co^{III} correspond to the species electrogenerated in a thin-layer spectroelectrochemical cell (see text for a discussion of the data).

Table 2. UV−Visible Spectral Data [λ_{max}, nm ($\epsilon \times 10^{-4}$ L mol^{-1} cm^{-1})] of Neutral and Electroreduced Iron Porphyrin−Corrole[a] Dyads in Pyridine Containing 0.1 M TBAP

		Soret region		Q region		
metal ions	macrocycle					$Co^{III}(py)_2$
Co^{III}	Me_4Ph_5Cor (**11**)		433 (3.5)		557 (0.7)	598 (1.7)
Fe^{III}	Et_2Me_6PhPor (**6**)	403 (15.7)		528 (1.2)		
Fe^{III}/Co^{III}	PCO (**7**)	404 (13.1)	436 (sh, 5.5)	529 (1.7)		599 (1.5)
	PCA (**8**)	407 (11.5)	437 (sh, 5.1)	528 (1.3)		601 (1.6)
	PCX (**9**)	404 (9.2)	434 (sh, 4.8)	528 (1.3)		600 (1.5)
	PCB (**10**)	371 (11.6)	395 (11.6)	527 (1.5)		none
Fe^{II}	Et_2Me_6PhPor (**6**)	313 (4.0)	413 (16.8)	519 (2.5)	549 (3.1)	
Fe^{II}/Co^{III}	PCO (**7**)	312 (5.0)	415 (13.9)[b]	521 (2.4)	551 (2.9)	599 (1.5)
	PCA (**8**)	313 (4.0)	412 (12.0)[b]	522 (1.8)	553 (2.1)	600 (1.6)
	PCX (**9**)	313 (4.0)	414 (12.0)[b]	521 (1.9)	552 (2.1)	600 (1.6)
	PCB (**10**)	313 (2.5)	412 (14.0)[b]	518 (0.6)	553 (1.3)	603 (1.7)

[a] Fe^{III} and Fe^{III}/Co^{III} represent the neutral compounds, while Fe^{II} and Fe^{II}/Co^{III} correspond to the species generated in a thin-layer spectroelectrochemical cell (see text for a discussion of the data). [b] A shoulder peak around 430 nm is overlapped by this band.

of the spacer. This is evaluated in the present paper, which illustrates for the first time the nonrigidity of the biphenylenyl (B) spacer for dyads containing axial ligands bound within the cavity of the two macrocycles and provides data on bis-macrocyclic systems that should be useful in future studies on molecular recognition.

Experimental Section

Instrumentation. Cyclic voltammetry was carried out with an EG&G model 173 potentiostat. A three-electrode system was used and consisted of a glassy carbon or platinum disk working electrode, a platinum wire counter electrode, and a saturated calomel reference electrode (SCE). The SCE was separated from the bulk of the solution by a fritted-glass bridge of low porosity that contained the solvent/supporting electrolyte mixture.

UV−visible spectroelectrochemical experiments were performed with an optically transparent platinum thin-layer electrode.[26] Potentials were applied with an EG&G model 173 potentiostat. Time-resolved UV−visible spectra were recorded with a Hewlett-Packard model 8453 diode array rapid-scanning spectrophotometer.

Measurement of Half-Wave Potentials. Three different techniques were used to measure half-wave potentials. Two of these involved "routine" cyclic voltammetry and thin-layer cyclic voltammetry where half-wave potentials were calculated as $E_{1/2} = (E_{pa} + E_{pc})/2$ and are referenced to SCE.

The Co^{III}/Co^{II} reaction investigated in this paper is sometimes not reversible on the routine cyclic voltammetry time scale of 0.1−0.5 V/s, and only broad "drawn out" peaks are obtained because of a potential-induced equilibrium between the bis- and mono-pyridine Co^{III} complexes in solution. Under these conditions, the values of $E_{1/2}$ could be obtained by the use of spectroelectrochemistry and of the Nernst equation, eq 1, where $[Co^{III}]$ represents the concentration of the cobalt(III) corrole in solution and $[Co^{II}]$ the concentration of the singly reduced species as determined from measurements of UV−visible spectra obtained during electroreduction.

$$E_{app} = E_{1/2} + (0.059/n)\log([Co^{III}]/[Co^{II}]) \quad (1)$$

The spectroelectrochemical method of evaluating $E_{1/2}$ involves collecting UV−visible spectra at a series of potentials on each side of the half-wave potential for the Co^{III}/Co^{II} process and then plotting the calculated value of E_{app} vs $\log([Co^{III}]/[Co^{II}])$ to obtain the thermodynamic half-wave potential. The theoretical slope of the E_{app} vs $\log([Co^{III}]/[Co^{II}])$ plot is 0.059 V for a one-electron transfer, and the intercept at $[Co^{III}] = [Co^{II}]$ provides an accurate measurement of $E_{1/2}$.

Ligand Binding Reactions Monitored by Electrochemistry. The binding of pyridine to the cobalt(III) corrole unit of the porphyrin−corrole dyads was carried out in benzonitrile (PhCN) at room temperature and monitored by electrochemistry. The determination of the pyridine binding constants followed methods described in the literature[27] and involved measurement of $E_{1/2}$ values as a function of the free ligand concentration and plots of $E_{1/2}$ vs log [py] using eq 2, where $(E_{1/2})_c$ is the half-wave potential for

(26) Lin, X. Q.; Kadish, K. M. *Anal. Chem.* **1985**, *57*, 1489−1501.

(27) (a) Crow, D. R. *Polarography of Metal Complexes*; Academic Press: London, 1969. (b) Kadish, K. M. In *Iron Porphyrins*; Lever, A. B. P., Gray, H. B., Eds.; Addison-Wesley Publishing Co.: London, 1983; Part II, pp 161−249.

Table 3. UV−Visible Spectral Data [λ_{max}, nm ($\epsilon \times 10^{-4}$ L mol^{-1} cm^{-1})] for (PCY)H_2Co Dyads in Pyridine

			Q region				
metal ions	macrocycle	Soret region					marker band[c]
2H	Et_2Me_6PhPor	404 (21.3)	502 (2.8)	534 (1.6)	572 (1.4)	625 (0.9)	
2H/Co^{III}	PCO	404 (25.2)[a]	504 (2.7)	535 (1.8)	573 (1.7)	*b*	599 (2.7)
	PCA	404 (17.5)[a]	504 (2.0)	538 (1.2)	573 (1.5)	*b*	602 (2.7)
	PCX	404 (17.9)[a]	504 (1.8)	534 (1.3)	574 (1.2)	*b*	602 (2.7)
	PCB	393 (16.6)[a]	504 (1.7)	531 (1.4)	575 (1.2)	622 (sh)[d]	none

[a] A shoulder around 430 nm is overlapped with this band. [b] This band is overlapped with the marker band at ~600 nm. [c] Diagnostic band for Co^{III}(py)$_2$. [d] sh = shoulder.

reduction of the complexed Co^{III}, $(E_{1/2})_s$ is the half-wave potential for reduction of the uncomplexed Co^{III}, $K_{Co(III)}$ is the formation constant (either K_1 or β_2) of interest, and p is the number of ligands bound to Co^{III}.

$$(E_{1/2})_c = (E_{1/2})_s - (0.059/n) \log K_{Co(III)} - (0.059/n) \log [py]^p \quad (2)$$

Chemicals and Reagents. The porphyrin−corrole dyads, (PCY)MClCoCl[19] and (PCY)H_2Co,[28,29] were synthesized according to previously described procedures. Absolute dichloromethane (CH_2Cl_2) was obtained from Fluka Chemical Co. and used as received. Pyridine (py) was obtained in high purity from Fluka, Aldrich, Sigma-Aldrich, or SDS and used as received or distilled over KOH pellets under argon and stored over 4 Å molecular sieves prior to use. No difference was observed in the electrochemical or spectroscopic data as a function of the source of pyridine or its degree of purification to remove any possible trace amines. PhCN was purchased from Aldrich Chemical Co. and distilled over P_2O_5 under vacuum prior to use. Tetra-*n*-butylammonium perchlorate (TBAP; Fluka Chemical Co.) was twice recrystallized from absolute ethanol and dried in a vacuum oven at 40 °C for 1 week prior to use.

Results and Discussion

UV−Visible Elucidation of the Metal Ion Oxidation State in (PCY)MClCoCl and (PCY)H_2Co. UV−visible spectroscopy was used to confirm the metal oxidation state of the cobalt corrole and iron, manganese, or free-base porphyrins in solutions of pyridine prior to electrochemical characterization. We have previously examined a number of cobalt mono-corroles,[30,31] bis-corroles,[15] and porphyrin−corrole dyads[16] having the same linker groups as those in the present study and have demonstrated that the presence of a visible absorption band at 598−601 nm in pyridine is an unambiguous "marker band" for a bis-pyridine cobalt(III) corrole, either in its monomeric form[30,31] or as part of a dyad containing a second face-to-face-linked macrocycle.[12,15,16] This 600 nm marker band is seen for all of the complexes with O, A, or X bridges in pyridine (Tables 1 and 2), and this implies a conversion of (PCY)M^{III}ClCo^{IV}Cl to its Co^{III} oxidation state upon dissolution of the dyad in neat pyridine. The dyads with B bridges also contain a cobalt(III) corrole in pyridine solutions, as shown by other data described in this paper.

The chemical conversion of a Co^{IV}Cl corrole dyad to its Co^{III} form in pyridine is not without precedent in the literature, and similar ligand-induced reductions have been reported for iron(III) porphyrins upon coordination with pyridine or other nitrogenous bases.[32] Indeed, the addition of OH^- to solutions of (TPP)Fe^{III}Cl (TPP = *meso*-tetraphenylporphyrin) in pyridine also induces a rapid stoichiometric reduction of the metal center by the axially bound pyridine molecule, giving rise to a porphyrin containing the Fe^{II} central metal ion. In the present work, we attempted to isolate a stable cobalt(IV) corrole dyad containing bound pyridine. However, this was not possible in the absence of an applied positive potential because of the very positive $E_{1/2}$ value of the Co^{IV}/Co^{III} process, which ranges between 0.23 and 0.37 V as described in a later section of the paper.

The oxidation state of the electrochemically examined manganese and iron porphyrins in the (PCY)MClCoCl dyads remains unchanged in pyridine from that which is observed in a nonbonding solvent such as CH_2Cl_2.[19] The manganese porphyrins of the examined dyads all have Mn^{III} UV−vis bands at 474−478 nm in pyridine, which are not observed in the case of electrogenerated manganese(II) porphyrins, with this latter oxidation state being characterized in pyridine by an intense Soret band at 429−432 nm (see Table 1). The spectroscopic bands that characterize the iron(III) and free-base porphyrins in pyridine are also unambiguous. As seen in Table 2, all of the dyads with iron(III) porphyrins have a single Q band at 527−529 nm, while all those with electrogenerated iron(II) porphyrins display two well-defined Q bands at 518−522 and 549−553 nm (see Table 3 and later discussion of spectroelectrochemical data). This contrasts with the free-base porphyrin/cobalt corrole dyads, which are characterized by four porphyrin absorption bands in the visible region of the spectrum (although the weakest of the bands at ~625 nm is hard to observe). Thus, the UV−visible data give clear evidence for dyads containing an iron(III) porphyrin, a manganese(III) porphyrin, or a free-base porphyrin linked to a cobalt(III) corrole in pyridine.

Under these solution conditions, the electrochemistry of the heterobimetallic dyads can be compared to that of (PCY)H_2Co^{III} because all of the derivatives contain a cobalt(III) corrole in neat pyridine. Despite this assignment of the oxidation state, the notation utilized in the paper for the heterobimetallic dyads is given as (PCY)MClCoCl, the species added to solution in each case.

(28) Barbe, J.-M.; Stern, C.; Pacholska, E.; Espinosa, E.; Guilard, R. *J. Porphyrins Phthalocyanines* **2004**, *8*, 301−312.
(29) Barbe, J.-M.; Burdet, F.; Espinosa, E.; Gros, C. P.; Guilard, R. *J. Porphyrins Phthalocyanines* **2003**, *7*, 365−374.
(30) Guilard, R.; Gros, C. P.; Bolze, F.; Jérôme, F.; Ou, Z.; Shao, J.; Fischer, J.; Weiss, R.; Kadish, K. M. *Inorg. Chem.* **2001**, *40*, 4845−4855.
(31) Kadish, K. M.; Shao, J.; Ou, Z. P.; Gros, C. P.; Bolze, F.; Barbe, J.-M.; Guilard, R. *Inorg. Chem.* **2003**, *42*, 4062−4070.
(32) (a) Srivatsa, G. S.; Sawyer, D. T. *Inorg. Chem.* **1985**, *24*, 1732−1734. (b) Brewer, C. *Inorg. Chim. Acta* **1988**, *150*, 189−192. (c) Epstein, L. M.; Straub, D. K.; Maricondi, C. *Inorg. Chem.* **1967**, *6*, 1720−1724.

Table 4. Half-Wave Potentials (V vs SCE) for Porphyrin−Corrole Dyads, (PCY)MCoCl (Where M = FeCl or MnCl) or (PCY)H_2Co, in Pyridine Containing 0.1 M TBAP

	oxidation	reduction		
compound	ring-centered	M^{III}/M^{II}	Co^{III}/Co^{II}	ring-centered
(Me_4Ph_5Cor)Co	0.27		−0.72[b]	−1.61
(Et_2Me_6PhPor)H_2	*a*			−1.36, −1.73
(PCO)H_2Co	0.28		−0.72[b]	−1.32, −1.59, −1.83
(PCA)H_2Co	0.26		−0.70	−1.36, −1.64, −1.72, −1.90
(PCX)H_2Co	0.23		−0.64	−1.36, −1.48, −1.68, −1.80
(PCB)H_2Co	0.31		−0.59	−1.36, −1.53, −1.76, −1.89
(Et_2Me_6PhPor)FeCl		−0.04		−1.81[d]
(PCO)FeClCoCl	0.35	−0.02	−0.68[c]	−1.60[e]
(PCA)FeClCoCl	0.31	−0.03	−0.72[b]	−1.64[e]
(PCX)FeClCoCl	0.30	−0.04−0.54[d]	−0.73[b]	−1.69[e]
(PCB)FeClCoCl	0.37	−0.02−0.54[d]	−0.71[b]	−1.67[e]
(Et_2Me_6PhPor)MnCl		−0.43		−1.57
(PCO)MnClCoCl	0.35	−0.42[b]	−0.70[b]	−1.59[e]
(PCA)MnClCoCl	0.33	−0.42[b]	−0.72[b]	−1.64[e]
(PCX)MnClCoCl	0.32	−0.42[b]	−0.72[b]	−1.68[e]
(PCB)MnClCoCl	0.49[d]	−0.44	−0.62	−1.62[e]

[a] Beyond the anodic potential limit of the solvent. [b] Obtained by spectroelectrochemical experiments. [c] Obtained by thin-layer cyclic voltammetry at a scan rate of 0.02 V/s. [d] Peak potential at a scan rate of 0.1 V/s. [e] Two overlapping one-electron processes.

Electroreduction of (PCY)H_2Co. The electrochemistry of (PCY)H_2Co^{III} in pyridine can be described as an overlapping of redox processes associated with the free-base porphyrin and the cobalt(III) corrole, the latter of which most closely resembles the well-studied (Me_4Ph_5Cor)Co.[31] The relevant monomeric porphyrin analogue is (Et_2Me_6PhPor)H_2 (see Chart 1), which structurally and electrochemically resembles free-base octaethylporphyrin, (OEP)H_2.

Thus, the "combined" data on (Et_2Me_6PhPor)H_2 (or its analogue, (OEP)H_2) and (Me_4Ph_5Cor)Co^{III} should provide a first approximation of the dyad's redox reactivity, with any differences between the two types of compounds (monomacrocycle and dyad) being attributed in part to interactions that exist between the two closely spaced macrocycles in solution and in part to differences in the axial ligand binding between the monomeric porphyrins or corroles and the related macrocycles in the dyad. The electroreduction of the four dyads is characterized by four- or five-electron-transfer processes in pyridine.

The first and third reductions involve the corrole part of the molecule, while the second and fourth involve the free-base porphyrin macrocycle, which is reduced in two steps to give a porphyrin π-anion radical and dianion. The potentials for these processes are as expected for cobalt mono-corroles[12,21,22] and free-base mono-porphyrins[20a,b] with similar structures, and these $E_{1/2}$ values are summarized in Table 4 along with data for the corresponding monomers. The electroreductions in Figure 1 at −1.80 to −1.90 V are close to the cathodic potential limit of the solvent and are unknown as to their origin.

The Co^{III}/Co^{II} process of corroles has been very well-characterized in the literature[12,21,22] and has been described in most detail[15,16,30,31,33] for macrocycles related to those in the present study. Specifically, all known four-coordinate cobalt(III) corroles are reversibly reduced at $E_{1/2}$ values of −0.15 to −0.38 V (depending upon the nature of the macrocycle substituents, the solvent, and the presence or absence of a second linked macrocycle),[15,16,30,31,33] while all known six-coordinate cobalt(III) corroles with axially bound pyridine are reduced at much more negative potentials.[31] The reduction of (Cor)$Co^{III}(py)_2$ to $[(Cor)Co^{II}]^-$, where Cor represents a general corrole macrocycle, is kinetically slow,[31] and thus different current−voltage curves will be observed by routine cyclic voltammetry (at scan rates of 0.1−1.0 V/s)

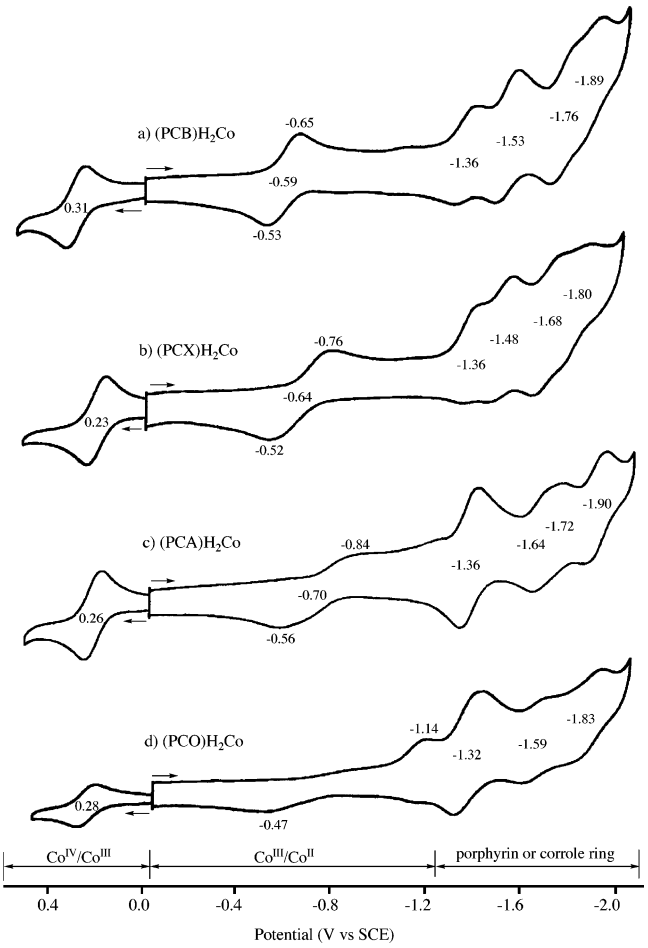

Figure 1. Cyclic voltammograms of (a) (PCB)H_2Co, (b) (PCX)H_2Co, (c) (PCA)H_2Co, and (d) (PCO)H_2Co in pyridine, 0.1 M TBAP.

(33) Kadish, K. M.; Adamian, V. A.; Van Caemelbecke, E.; Gueletii, E.; Will, S.; Erben, C.; Vogel, E. *J. Am. Chem. Soc.* **1998**, *120*, 11986−11993.

and thin-layer cyclic voltammetry, where the scan rate is much slower, usually 5−20 mV/s. The measured value of E_p for the one-electron reduction of $(Cor)Co^{III}(py)_2$ in neat pyridine can be as negative as −1.10 to −1.20 V vs SCE by routine cyclic voltammetry, but the thermodynamic $E_{1/2}$ value, as determined by thin-layer UV−visible spectroelectrochemistry, ranges from $E_{1/2} = -0.70$ to −0.75 V depending upon the macrocycle.[31]

The electrochemistry of five-coordinate cobalt(III) corroles has not previously been described in the literature for monocorroles of the type investigated in the present study (see Chart 1), but a cobalt(III) phosphine adduct has been reported[34] and two additional examples of five-coordinate cobalt(III) corroles are given in the present paper for compounds having the B bridge. One of these examples is $(PCB)H_2Co(py)$, which has been structurally characterized in the solid state[29] and which undergoes a quasi-reversible reduction to Co^{II} at −0.59 V vs SCE (see Figure 1a). The Co^{III}/Co^{II} processes of $(PCX)H_2Co$ and $(PCA)H_2Co$ are also quasi-reversible, and these one-electron reductions occur at −0.64 and −0.70 V, respectively, with $|E_{pa} - E_{pc}|$ values of 0.24 and 0.38 V for a scan rate of 0.1 V/s (Figure 1b,c). This contrasts with what is observed in the case of $(PCO)H_2Co$, where the Co^{III}/Co^{II} reduction is irreversible by routine cyclic voltammetry with $E_{pc} = -1.14$ V and $E_{pa} = -0.47$ V for a scan rate of 0.1 V/s (Figure 1d). This clearly indicates the formation of a six-coordinate Co^{III} species in the dyad, i.e., $(PCO)H_2Co(py)_2$.

The trend in reversibility for the Co^{III}/Co^{II} reaction as described by the peak-to-peak separation in Figure 1 directly parallels the spacer size in the different dyads, i.e., PCB < PCX < PCA < PCO, and this is also related to the number of pyridine molecules inside the cavity that are bound to Co^{III}. The Co^{III} center of $(PCB)H_2Co$ binds a single pyridine ligand in the solid state[29] as well as in solution, as shown by an electrochemically monitored titration of the Co^{III}/Co^{II} process using equations described in the literature for reduction of the mono-corrole, $(Me_4Ph_5Cor)Co$, in PhCN/pyridine mixtures.[31]

Cobalt(II) corroles do not bind pyridine ligands,[12,21,31] and thus a plot of $E_{1/2}$ vs log [py] for the Co^{III}/Co^{II} process of the dyads in PhCN/pyridine mixtures should have a slope of −0.118 V for the reduction of $Co^{III}(py)_2$ to Co^{II} and −0.059 V for the reduction of $Co^{III}(py)$ to Co^{II}. An example of such a diagnostic plot is shown in Figure 2a for the case of $(PCB)H_2Co$. The slope of the plot is −0.059 V from log [py] = −3.5 to −0.5, consistent with the binding of one pyridine ligand to the initial dyad, giving $(PCB)H_2Co^{III}(py)$ and its reduction to $[(PCB)H_2Co^{II}]^-$ with loss of the axial ligand, as indicated by the Nernstian (−0.059 V) slope of the plot in Figure 2. The log [py] = 0 intercept of the plot, when combined with $E_{1/2}$ in the absence of pyridine coordination, enables a calculation of the pyridine binding constant to $(PCB)H_2Co$ using equations in the literature[27] and gives an experimentally measured log $K = 3.6$.

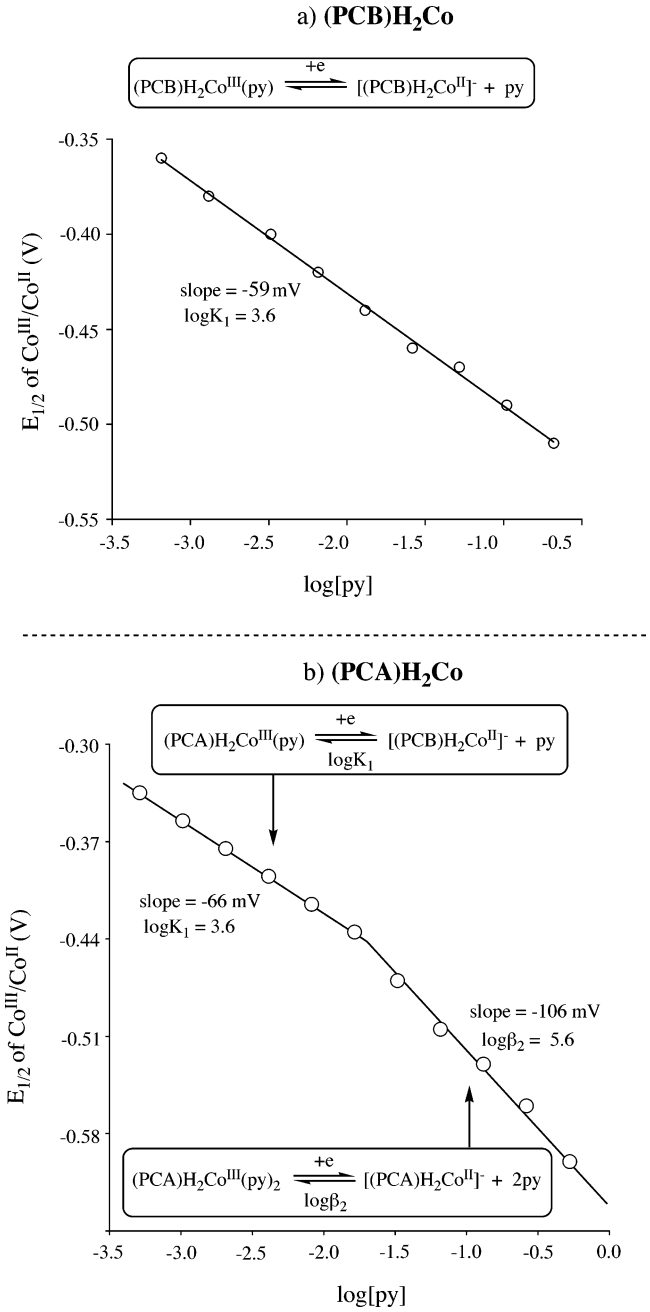

Figure 2. $E_{1/2}$ vs log [py] for the Co^{III}/Co^{II} processes of (a) $(PCB)H_2Co$ (top) and (b) $(PCA)H_2Co$ (bottom) in PhCN, 0.1 M TBAP.

In contrast, $(PCX)H_2Co$ has been characterized as a bis-pyridine adduct, $(PCX)H_2Co(py)_2$, in the solid state,[28] while $(PCA)H_2Co$ and $(PCX)H_2Co$ exist as a mixture of five- and six-coordinate cobalt(III) pyridine adducts in pyridine solutions, the latter of which is predominant under the electrochemically investigated conditions. Pyridine binding constants were also calculated for these two dyads in PhCN using the method of calculation described above for $(PCB)H_2Co$. An example of the $E_{1/2}$ vs log [py] plot is also shown in Figure 2b for $(PCA)H_2Co$ and gives values of log K_1 and log β_2 of 3.6 and 5.6, respectively.

In summary, the electrochemical and spectroscopic data indicate that the free-base porphyrin dyad with the shortest spacer, PCB, is linked to a five-coordinate cobalt(III) corrole,

(34) Kadish, K. M.; Koh, W.; Tagliatesta, P.; Sazou, D.; Paolesse, R.; Licoccia, S.; Boschi, T. *Inorg. Chem.* **1992**, *31*, 2305−2313.

Scheme 2. Co^{III}/Co^{II} Processes of $(PCY)H_2Co^{III}$ in Pyridine

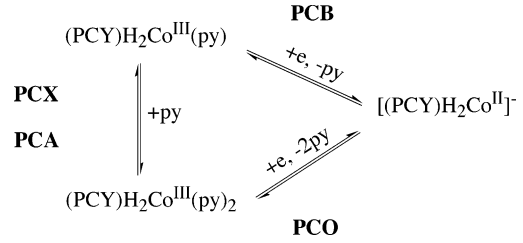

giving $(PCB)H_2Co(py)$ in pyridine, while the dyad with the largest spacer, PCO, is linked to a six-coordinate cobalt(III) corrole, giving $(PCO)H_2Co(py)_2$. The other two investigated dyads, PCA and PCX, exist as a mixture of the five- and six-coordinate Co^{III} complexes in pyridine. None of the cobalt(II) corroles bind pyridine axial ligands, and thus the electroreduction for $(PCY)H_2Co$ proceeds as shown in Scheme 2.

Electrochemistry of (PCY)FeClCoCl. Figure 3 shows cyclic voltammograms of three (PCY)FeClCoCl dyads (PCB, PCX, and PCO) and the related monomeric units in pyridine containing 0.1 M TBAP. The half-wave potentials for each reaction are given in Table 4, which also includes data for (PCA)FeClCoCl, which is not shown in the figure. The UV−visible spectra of the PCO, PCA, and PCX complexes indicate that the corrole unit in these dyads is converted to its Co^{III} form upon dissolution of the compounds in neat pyridine, and thus the electrode reactions in Figure 3 pertain to dyads containing a linked iron(III) porphyrin and a cobalt(III) corrole rather than an Fe^{III}/Co^{IV} complex, which exists in CH_2Cl_2 or PhCN.[19] These compounds are then electroreduced as shown in Scheme 1.

No oxidations are observed for the monomeric iron(III) porphyrin, $(Et_2Me_6PhPor)FeCl$, up to the anodic potential limit of pyridine (~0.8 V), but the three expected[20a,b] one-electron reductions can be observed for this complex (see Figure 3d). The first and third reductions are reversible with $E_{1/2} = -0.04$ and -1.91 V, while the second is irreversible with $E_{pc} = -1.80$ V for a scan rate of 0.1 V/s. The redox behavior of $(Et_2Me_6PhPor)FeCl$ in pyridine is comparable to what has been reported for (OEP)FeCl[35] and (TPP)FeCl (TPP = tetraphenylporphyrin dianion),[20a,b] each of which axially binds two pyridine ligands in neat pyridine or pyridine/CH_2Cl_2 mixtures. A similar ligand binding reaction occurs for $(Et_2Me_6PhPor)FeCl$, resulting in the formation of $[(Et_2Me_6PhPor)Fe^{III}(py)_2]^+Cl^-$, which is reversibly reduced at $E_{1/2} = -0.04$ V to give $(Et_2Me_6PhPor)Fe^{II}(py)_2$. The assignment of two pyridine ligands on both Fe^{III} and Fe^{II} is thus consistent with the results in the literature for related porphyrins that have been examined in pyridine,[36,37] and it also agrees with spectroelectrochemistry data discussed in later sections of this paper.

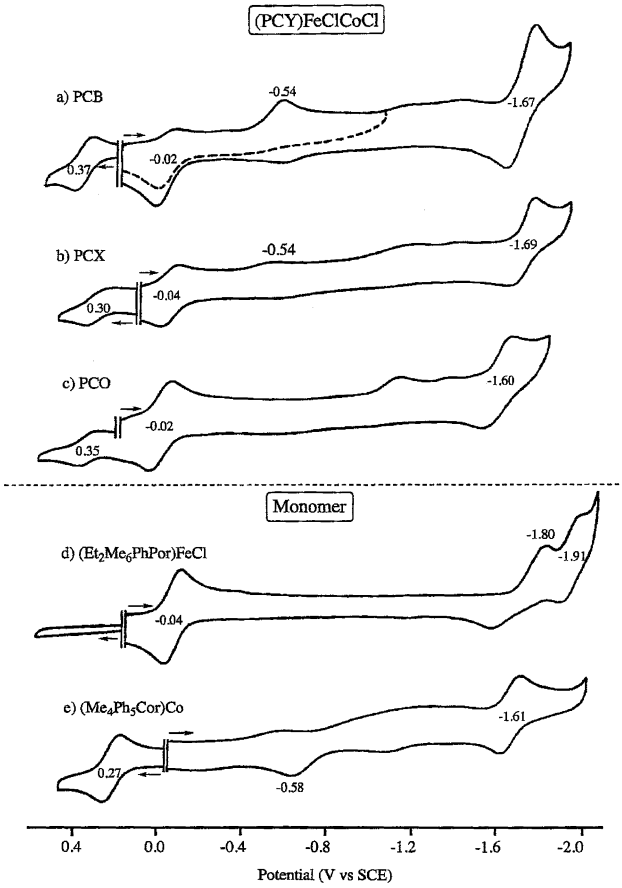

Figure 3. Cyclic voltammograms of (a) (PCB)FeClCoCl, (b) (PCX)-FeClCoCl, (c) (PCO)FeClCoCl, (d) $(Et_2Me_6PhPor)FeCl$, and (e) $(Me_4Ph_5Cor)Co$ in pyridine containing 0.1 M TBAP.

Iron(I) porphyrins show no coordination in pyridine at room temperature,[20a,b] and thus the further reduction of $(Et_2Me_6PhPor)Fe^{II}(py)_2$ at $E_p = -1.80$ V is accompanied by a dissociation of the two axially bound pyridine ligands. The third reduction of the iron porphyrin in pyridine is macrocycle-centered and generates an Fe^{I} π-anion radical.[20a,b]

The Fe^{III}/Fe^{II} redox processes of the porphyrin−corrole dyads, (PCY)FeClCoCl, occurs at $E_{1/2} = -0.02$ to -0.04 V in pyridine (see Figure 3a−c and Table 4), and these half-wave potentials are virtually identical with the measured $E_{1/2}$ (-0.04 V) for reduction of $[(Et_2Me_6PhPor)Fe^{III}(py)_2]^+$ to give $(Et_2Me_6PhPor)Fe^{II}(py)_2$ (Figure 3d). The fact that the first reduction potentials of (PCO)FeClCoCl, (PCA)FeClCoCl, and (PCX)FeClCoCl show no differences in $E_{1/2}$ compared with the related iron(III) mono-porphyrin indicates that the cobalt corrole macrocycle in these three porphyrin−corrole dyads has little or no effect on the Fe^{III}/Fe^{II} process under these solution conditions (see Table 4).

(PCB)FeClCoCl also undergoes a reversible Fe^{III}/Fe^{II} reduction at $E_{1/2} = -0.02$ V, but an additional irreversible Fe^{III} reduction is also observed at $E_{pc} = -0.54$ V for a scan rate of 0.1 V/s (Figure 3a). The behavior of (PCB)FeClCoCl also differs from that of (PCO)FeClCoCl, (PCX)FeClCoCl, and (PCA)FeClCoCl in that the ratio of cathodic to anodic peak currents for the first reduction (i_{pc1}/i_{pa1}) is smaller than that in the case of an uncomplicated Nernstian process where

(35) Kadish, K. M.; Tabard, A.; Lee, W.; Liu, Y. H.; Ratti, C.; Guilard, R. *Inorg. Chem.* **1991**, *30*, 1542−1549.
(36) Kadish, K. M.; Bottomley, L. A. *J. Am. Chem. Soc.* **1977**, *99*, 2380−2382.
(37) Kadish, K. M.; Van Caemelbecke, E.; D'Souza, F.; Lin, M.; Nurco, D. J.; Medforth, C. J.; Forsyth, T. P.; Krattinger, B.; Smith, K. M.; Fukuzumi, S.; Nakanishi, I.; Shelnutt, J. A. *Inorg. Chem.* **1999**, *38*, 2188−2198.

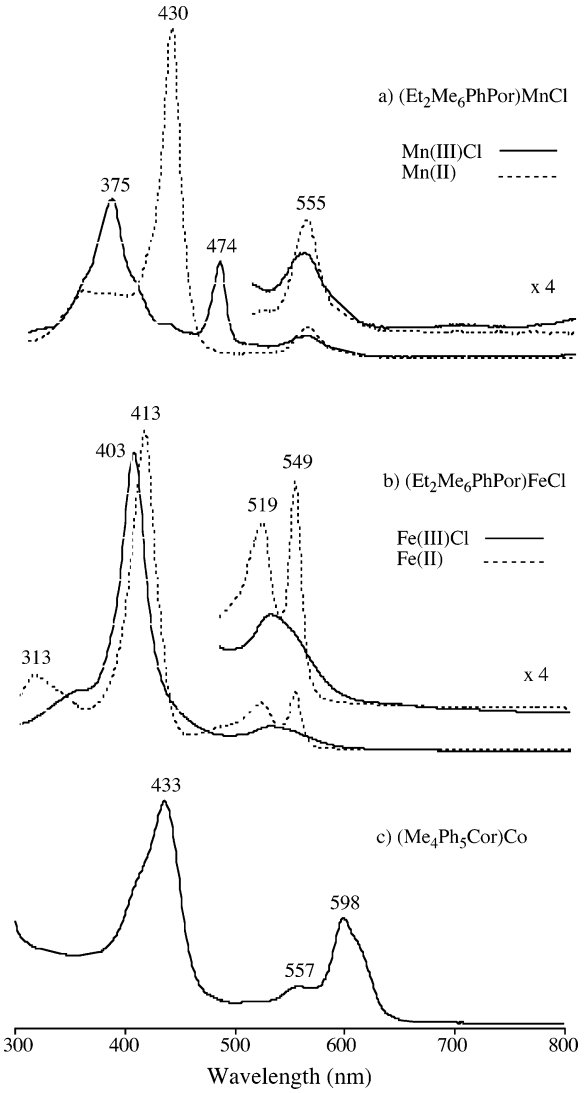

Figure 4. UV−visible spectra of (a) $(Et_2Me_6PhPor)MnCl$ (solid line) and the singly reduced species (dashed line), (b) $(Et_2Me_6PhPor)FeCl$ (solid line) and the singly reduced species (dashed line), and (c) $(Me_4Ph_5Cor)Co(py)_2$ in pyridine, 0.1 M TBAP.

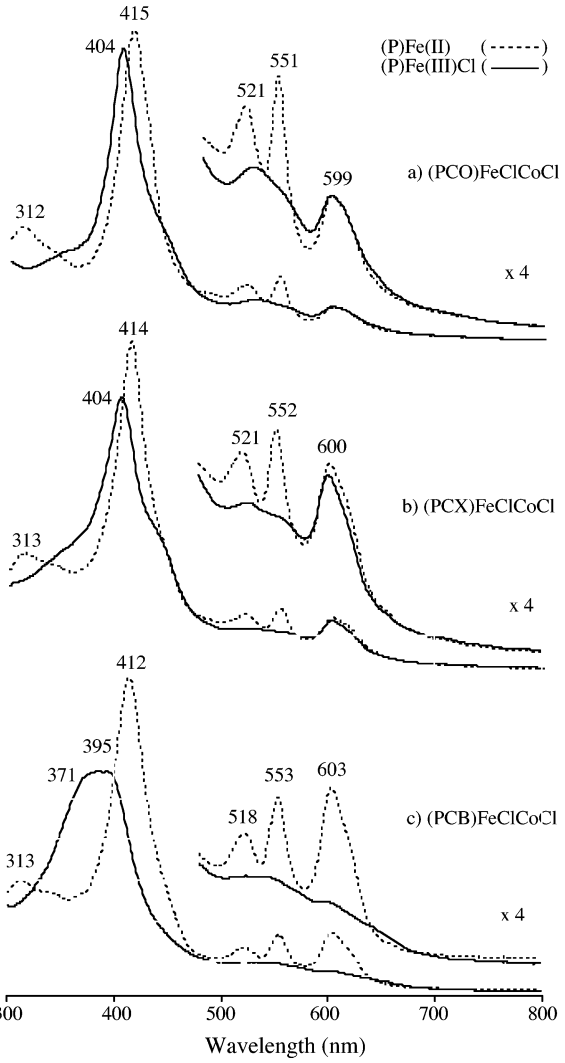

Figure 5. UV−visible spectra of (PCY)FeClCoCl (solid line) and the singly reduced species (dashed line) in pyridine, 0.1 M TBAP, where Y = O, X, and B.

$i_{pc}/i_{pa} = 1$. An irreversible reduction at $E_p = -0.54$ V can also be seen for (PCX)FeClCoCl (Figure 3b and Table 4), but the current height of this process (i_{pc2}) is significantly lower than that of the first reduction (i_{pc1}) at $E_{1/2} = -0.04$ V. (PCO)FeClCoCl (Figure 3c) and (PCA)FeClCoCl (figure not shown) do not exhibit an irreversible Fe^{III} reduction at $E_p = -0.54$ V.

The fact that (PCB)FeClCoCl undergoes a well-defined reduction at $E_p = -0.54$ V in neat pyridine indicates that the anionic Cl^- ligand remains bound to the Fe^{III} center prior to electroreduction because the bis-pyridine adduct is characterized by a reduction potential of −0.02 to −0.04 V. Half-wave potentials of −0.50 to −0.51 V have been reported for the reduction of (OEP)FeCl in a variety of nonbonding solvents[20,38] and indicate that the reduction of (PCB)FeClCoCl proceeds via an $Fe^{III}Cl/Fe^{II}$ process, after which the iron(II) bis-pyridine adduct is rapidly formed in solution, as was described in detail for the case of (TPP)FeCl in pyridine.[36,37]

In contrast to what is observed for (PCB)FeClCoCl, the electrochemical data indicate that the Fe^{III} centers of (PCO)FeClCoCl and (PCA)FeClCoCl both contain two axially coordinated pyridine molecules prior to electroreduction, while UV−visible data of the initial compounds (Table 2) show that two pyridine molecules are also bound to the Co^{III} center of the corrole in these two dyads. This latter fact is indicated by the presence of a diagnostic 600 nm marker band for the PCO and PCA dyads whose molar absorptivities (ϵ) are virtually the same as those for the monocorrole in neat pyridine, which has earlier been characterized as a bis-pyridine adduct in the solid state[30] and in solution.[16] The $Co^{III}(py)_2$ assignment is also shown by the lack of a reversible Co^{III}/Co^{II} process for the PCO and PCA derivatives, which has been described earlier as a diagnostic criterion for bis-pyridine adducts of cobalt(III) corroles[31] and is also observed for $(PCO)H_2Co$ in pyridine (Figure 1d).

Quite different axial coordination is seen for (PCB)FeClCoCl in pyridine, where the electrochemistry

(38) Guilard, R.; Boisselier-Cocolios, B.; Tabard, A.; Cocolios, P.; Simonet, B.; Kadish, K. M. *Inorg. Chem.* **1985**, *24*, 2509−2520.

(Figure 3a) indicates little or no binding of pyridine to the Fe^{III} center while the UV−visible data (Table 2) indicate the lack of a six-coordinate cobalt(III) corrole. Thus, two different extremes of pyridine coordination are present in the initial electroactive form of this dyad. One is in $[(PCY)Fe^{III}(py)_2Co^{III}(py)_2]^+$, which contains four bound pyridine molecules when Y = O or A, and the other is in $(PCB)Fe^{III}ClCo^{III}(py)$, which contains only a singly coordinated pyridine molecule. (PCX)FeClCoCl has behavior between the two extremes but, like the other three dyads, is reduced to an Fe^{II}/Co^{III} derivative containing four axially coordinated pyridine molecules, as is described by the spectroelectrochemistry discussed below.

Spectroelectrochemistry of (PCY)FeClCoCl and Elucidation of Reduction Mechanisms. The electron-transfer mechanisms for the iron porphyrin dyads can be assigned on the basis of electrochemical and UV−visible data when compared to the corresponding monomeric units. The monomeric iron(III) porphyrin in pyridine exhibits an intense Soret band at 403 nm and a broad visible band at 528 nm (solid line in Figure 4b), which is assigned to the six-coordinated bis-pyridine adduct, $[(Et_2Me_6PhPor)Fe^{III}(py)_2]^+Cl^-$. The neutral porphyrin−corrole dyads, (PCO)FeClCoCl (Figure 5a), (PCX)FeClCoCl (Figure 5b), and (PCA)FeClCoCl (Table 2), display quite similar spectra, with an Fe^{III} Soret band at 404−407 nm and a broad visible band at 527−529 nm (Table 2). The spectra of the dyads are almost superimposable with the spectrum of the corresponding iron(III) porphyrin monomer (Figure 4b), with the exception of a shoulder at 434−437 nm and a weak visible band at 599−601 nm, both of which originate from the cobalt corrole macrocycle in the dyads (see Figure 4c for the spectrum of $(Me_4Ph_5Cor)Co$ in pyridine).

A quite different UV−visible spectrum is seen for (PCB)FeClCoCl in pyridine. This spectrum is shown in Figure 5c and is characterized by a broad Soret band at 371−395 nm (rather than at 404−407 nm), and there is no 600 nm $Co^{III}(py)_2$ marker band, as is seen for the other three (PCY)FeClCoCl derivatives in pyridine (Table 2). These spectral differences between the PCB dyad and the other three Fe^{III} dyads can be attributed in part to the fact that there is a stronger interaction between the two macrocycles in the PCB complex, in part to the fact that Cl^- remains bound to the Fe^{III} center of the PCB derivative (as ascertained by the irreversible reduction of Fe^{III} at $E_p = -0.54$ V), and in part to the lack of pyridine binding inside the cavity of (PCB)FeClCoCl. The absence of a cobalt(III) bis-pyridine adduct is described above for $(PCB)H_2Co$, and this lack of a six-coordinate cobalt(III) corrole is also seen for the Mn^{III} form of (PCB)MnClCoCl, as discussed in a later section of the paper.

Despite differences in the UV−visible spectra between (PCB)FeClCoCl and the other three Fe^{III} dyads in pyridine, the same spectral pattern (and the same degree of axial pyridine coordination) is seen upon electroreduction to give the Fe^{II} form of the dyad. This is evident from a comparison of the UV−visible spectra in the reduced dyads in Figure 5 (dashed lines) with the spectrum for the Fe^{II} form of the

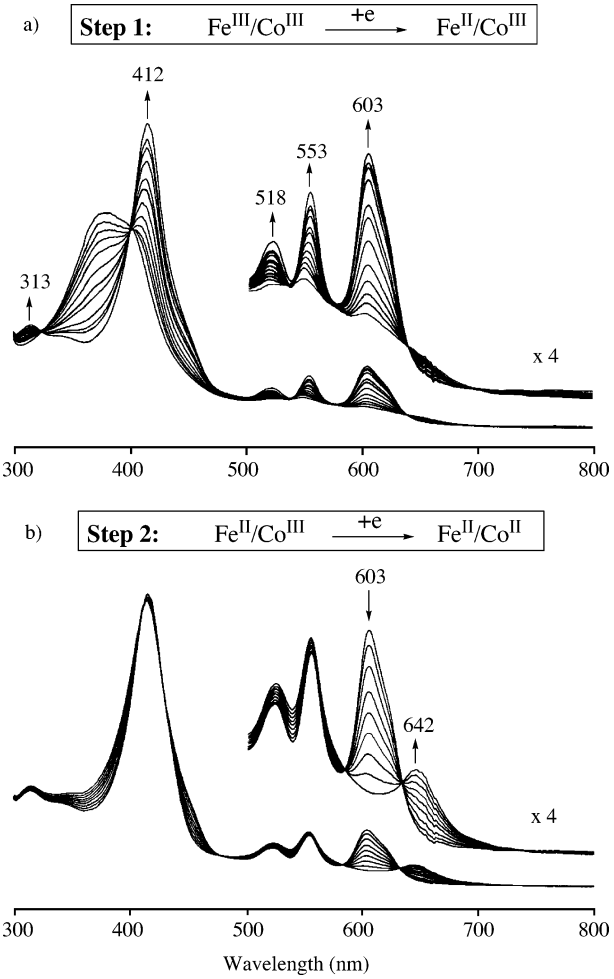

Figure 6. UV−visible spectra of (PCB)FeClCoCl at different applied potentials (a) from 0.0 to −0.6 V and (b) from −0.6 to −0.9 V in pyridine containing 0.1 M TBAP.

porphyrin monomer in Figure 4b. The wavelengths and molar absorptivities of these iron(III) and iron(II) porphyrin complexes are summarized in Table 2, which lists the spectral data of each neutral and singly reduced (PCY)FeClCoCl dyad.

As seen in the table and figures, all of the iron(II) porphyrins have an intense Soret band at 412−415 nm and two well-defined Q bands at 518−522 and 549−553 nm. The four dyads and $(Me_4Ph_5Cor)Co(py)_2$ (but not the Fe^{II} monomer) also all have a $Co^{III}(py)_2$ absorption band at 599−603 nm whose molar absorptivity ranges from 1.5×10^4 to 1.7×10^4. Virtually the same molar absorptivities are seen for the 600 nm band of unreduced (PCY)FeClCoCl where Y = O, A, or X (see Figure 5 and Table 2), thus indicating that there are two pyridine molecules on Co^{III} both before and after electroreduction of the iron(III) porphyrin to its Fe^{II} form.

The binding of two pyridine molecules to Co^{III} was totally unexpected for the PCB derivative, where the overall electrode reaction can be written as shown in eq 3.

$$(PCB)Fe^{III}ClCo^{III}(py) + e + 3py \xrightarrow{E_p = -0.54\ V} (PCB)Fe^{II}(py)_2Co^{III}(py)_2 \quad (3)$$

Scheme 3. Electroreduction Mechanisms for Dyads with Iron(III) Porphyrins

(PCY)FeClCoCl (Y = O, A and X)

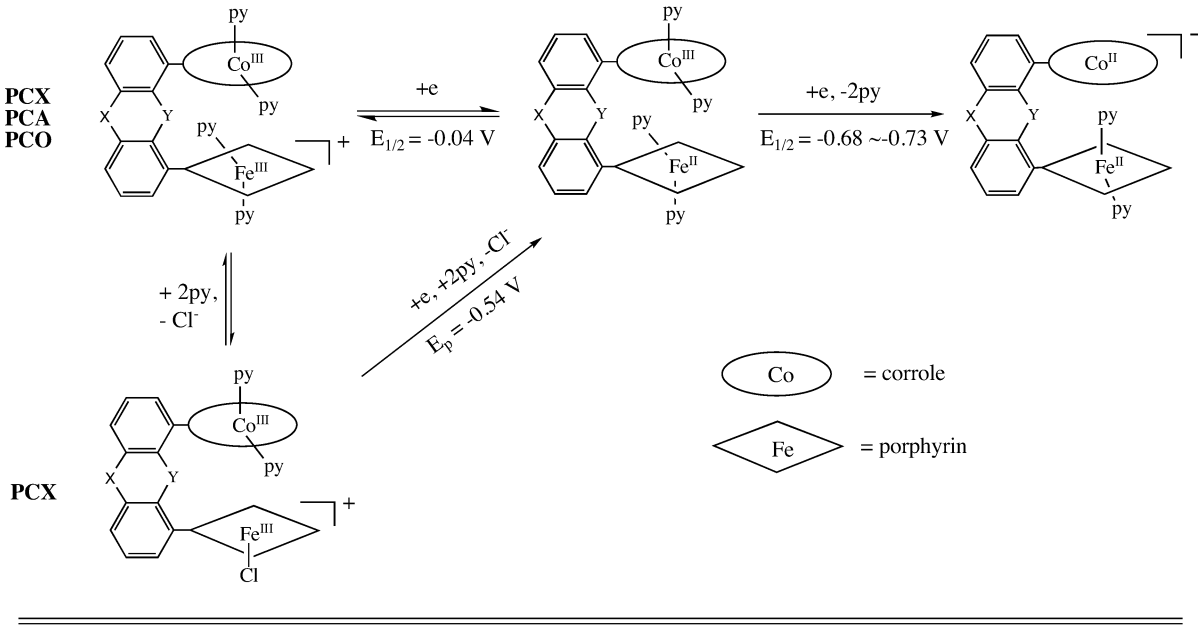

(PCB)FeClCoCl

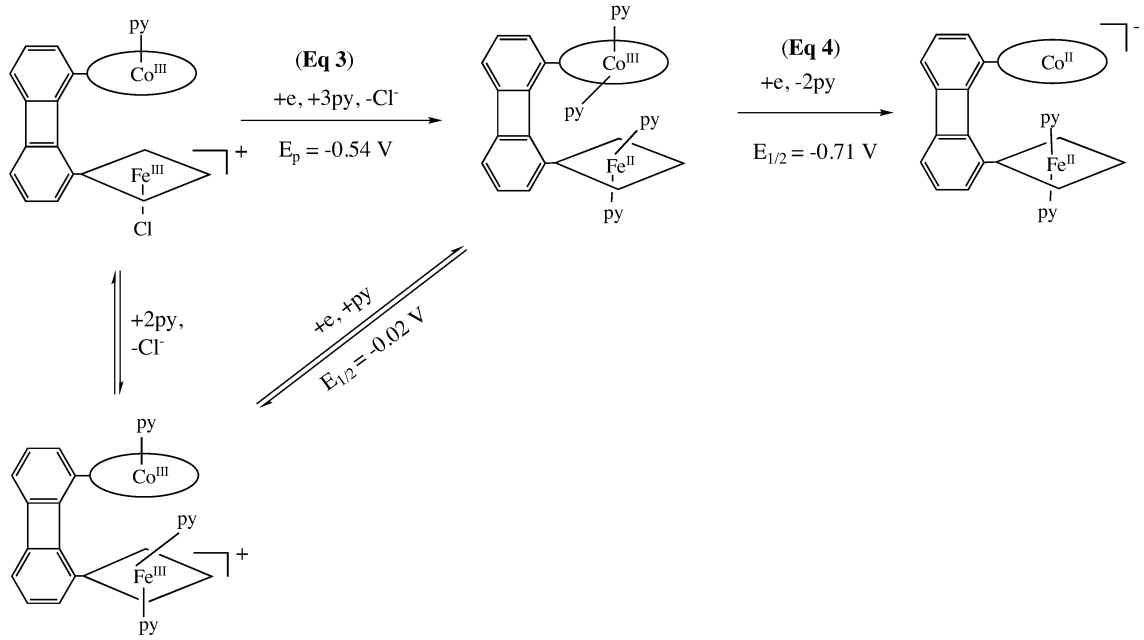

A further reduction of (PCB)$Fe^{II}(py)_2Co^{III}(py)_2$ to its Fe^{II}/Co^{II} form involves the loss of two pyridine ligands and proceeds via eq 4.

$$(PCB)Fe^{II}(py)_2Co^{III}(py)_2 + e \rightleftharpoons [(PCB)Fe^{II}(py)_2Co^{II}]^- + 2py \quad (4)$$

Evidence for the reaction sequence in eqs 3 and 4 is given in Figure 6. In the first one-electron reduction of (PCB)$Fe^{III}ClCo^{III}$(py) (eq 3 and step 1), the UV−visible bands for the electrogenerated $Fe^{II}(py)_2$ product at 412, 518, and 553 nm grow in, as does the diagnostic $Co^{III}(py)_2$ marker band at 603 nm. Isobestic points are obtained at 398 and 638 nm, indicating the lack of any spectrally detectable intermediates in the irreversible reduction that involves a loss of Cl^- and the addition of three pyridine molecules to the two metal centers. Isobestic behavior is also seen during the electroreduction of (PCB)$Fe^{II}(py)_2Co^{III}(py)_2$ to (PCB)$[Fe^{II}(py)_2Co^{II}]^-$ (eq 4 and step 2), where the 603 nm band disappears and is replaced by a 642 nm band, which

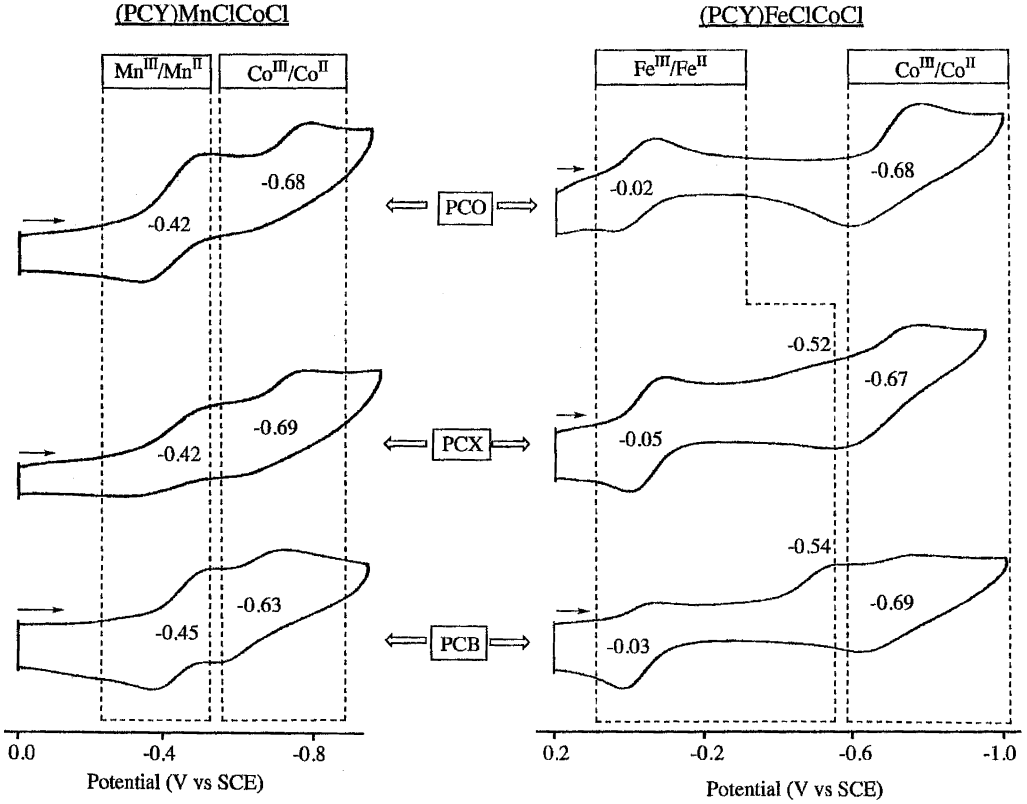

Figure 7. Comparative thin-layer cyclic voltammograms of (PCY)FeClCoCl and (PCY)MnClCoCl in pyridine containing 0.1 M TBAP.

was previously assigned to a four-coordinate cobalt(II) corrole in both bonding and nonbonding media including pyridine.[31] This leads to the overall electroreduction mechanisms shown in the top of Scheme 3 for (PCY)FeClCoCl, where Y = O, A, or X, and the bottom of Scheme 3 for (PCB)FeClCoCl.

Despite the irreversible nature of the Co^{III}/Co^{II} reduction in Figure 3a, a thermodynamic half-wave potential for this redox process of $(PCB)Fe^{II}(py)_2Co^{III}(py)_2$ (eq 4) can be obtained by the use of thin-layer electrochemistry (Figure 7) or thin-layer spectroelectrochemistry,[31] and an application of this latter method is illustrated in Figure 8, which analyzes the decrease in absorption of the 603 nm band for $Co^{III}(py)_2$ in Figure 6b as a function of the applied potential. The relative ratio of $[Co^{III}]/[Co^{II}]$ in the PCB dyad is determined by the relative intensity of the 603 nm band, and a plot of E_{app} vs $\log([Co^{III}]/[Co^{II}])$ gives a straight line slope of 0.059 V, as shown in Figure 8b. This Nernstian slope corresponds to a reversible one-electron reduction and gives an $E_{1/2} = -0.71$ V for the Co^{III}/Co^{II} process of (PCB)FeClCoCl. A similar method was used to calculate thermodynamic $E_{1/2}$ values for the Co^{III}/Co^{II} process of the other (PCY)FeClCoCl and (PCY)MnClCoCl dyads (see the following section). These half-wave potentials are summarized in Table 4 and range from -0.62 to -0.73 V. Almost identical values of $E_{1/2}$ are obtained from the thin-layer cyclic voltammograms, as seen in Figure 7.

Electrochemistry and Spectroelectrochemistry of (PCY)MnClCoCl in Pyridine. Cyclic voltammograms of (PCB)MnClCoCl, (PCX)MnClCoCl, and (PCO)MnClCoCl in pyridine are shown in Figure 9 along with those of monomeric $(Et_2Me_6PhPor)MnCl$ and $(Me_4Ph_5Cor)Co$. The measured half-wave potentials are summarized in Table 4, which also includes $E_{1/2}$ values for the reduction of (PCA)MnClCoCl, which is not illustrated in the figure.

The first two reductions of (PCB)MnClCoCl are reversible and located at $E_{1/2} = -0.44$ and -0.62 V vs SCE (Figure 9a). The -0.44 V value is virtually identical with $E_{1/2}$ for the first reduction of $(Et_2Me_6PhPor)MnCl$ in pyridine (Table 4 and Figure 9d) and is assigned as a Mn^{III}/Mn^{II} process. This reaction has been investigated in the literature for a large number of monomeric manganese porphyrins in pyridine,[20,39−41] and the electrode reduction has generally been assigned as $Mn^{III}(py)_2/Mn^{II}(py)$.

The second reduction of (PCB)MnClCoCl, at $E_{1/2} = -0.62$ V, occurs on the cobalt corrole center. The half-wave potential and reversibility of this reaction is comparable to that of the $(PCB)H_2Co$ dyad ($E_{1/2} = -0.59$ V, Figure 1a), which is attributed to a $Co^{III}(py)/Co^{II}$ process on the basis of electrochemical and spectroelectrochemical data discussed earlier in the paper.

The cyclic voltammogram of (PCB)MnClCoCl differs from the voltammograms of (PCX)MnClCoCl (Figure 9b), (PCO)MnClCoCl (Figure 9c), and (PCA)MnClCoCl (Table 4) in that an irreversible to quasi-reversible Mn^{III} reduction is obtained for the latter three dyads. In addition, the

(39) Guilard, R.; Jagerovic, N.; Barbe, J.-M.; Liu, Y. H.; Perrot, I.; Naillon, C.; Van Caemelbecke, E.; Kadish, K. M. *Polyhedron* **1995**, *14*, 3041−3050.
(40) Guilard, R.; Perié, K.; Barbe, J.-M.; Nurco, D. J.; Smith, K. M.; Van Caemelbecke, E.; Kadish, K. M. *Inorg. Chem.* **1998**, *37*, 973−981.
(41) Kelly, S. L.; Kadish, K. M. *Inorg. Chem.* **1982**, *21*, 3631−3639.

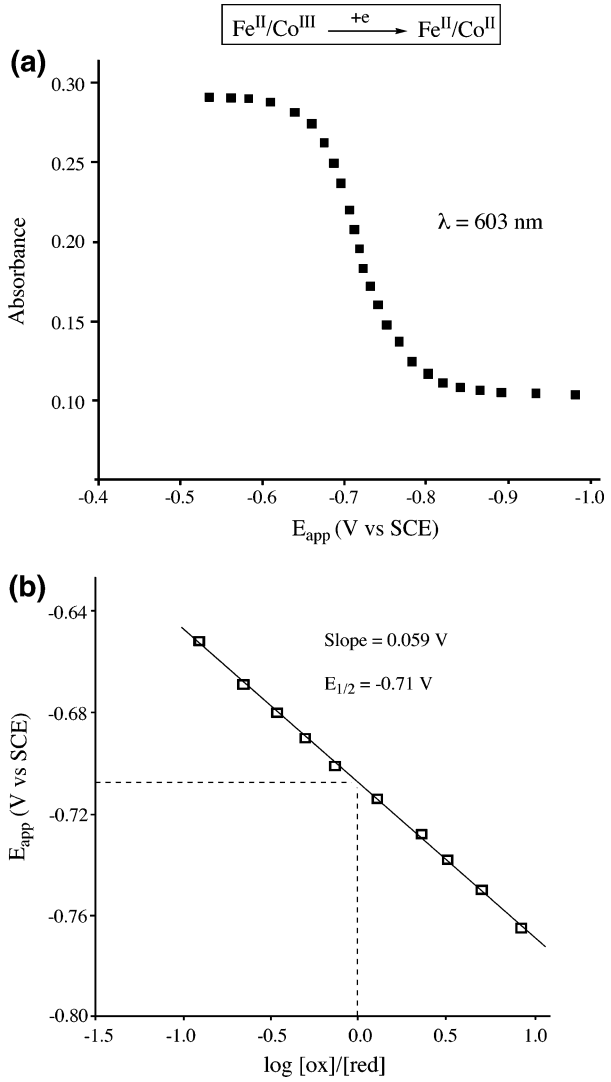

Figure 8. (a) Absorbance vs applied potentials (E_{app}) and (b) log([ox]/[red]) vs E_{app} for the Co^{III}/Co^{II} process of (PCB)FeClCoCl.

cobalt(III) corrole reduction is irreversible and ill-defined in (PCY)MnClCoCl, where Y = O, A, or X, but well-defined in (PCB)MnClCoCl.

As in the case of (PCY)FeClCoCl, the UV−visible spectra can be used to ascertain the degree of pyridine binding to the Co center of the dyad before and after electroreduction. This is shown by a comparison of the spectrum of the Mn^{III} monomer in Figure 4a with that of the manganese(III) porphyrin dyads in Figure 10. The monomeric manganese(III) porphyrin in pyridine exhibits an intense Soret band at 375 nm, a shoulder at 396 nm, and an additional band in the Soret region at 474 nm. A single Q band at 553 nm is also seen for this complex. (PCO)MnClCoCl, (PCX)MnClCoCl, and (PCA)MnClCoCl (Figure 10 and Table 1) show similar spectral features assigned to the manganese(III) porphyrin in pyridine. (PCX)MnClCoCl has bands at 373, 407, 475, and 554 nm (Figure 10b), while (PCO)MnClCoCl has bands at 377, 399, 474, and 554 nm (Figure 10a; see a summary of λ_{max} and ϵ in Table 1). The spectra of both dyads have a shoulder at around 420 nm and a Q band at 600 nm, the latter of which

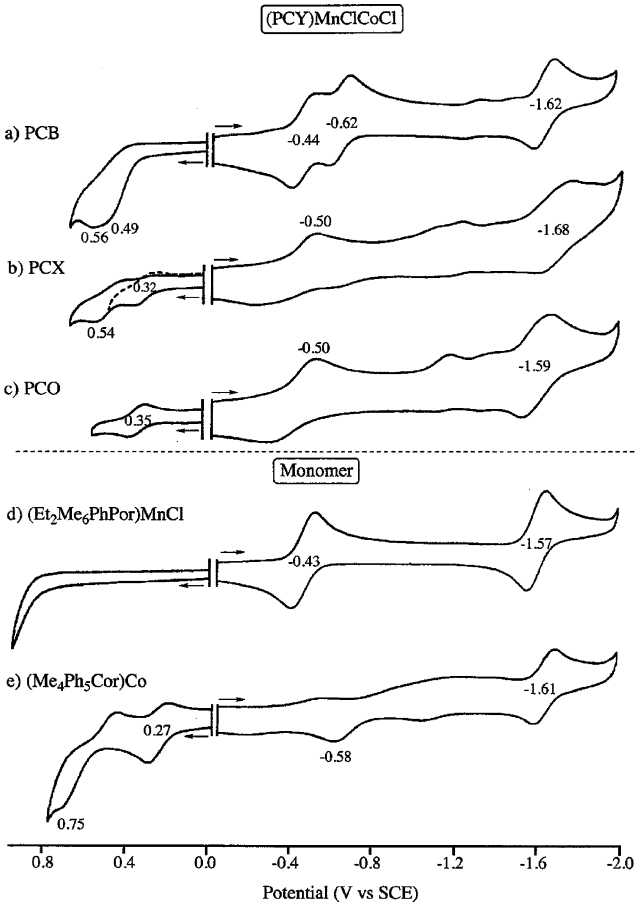

Figure 9. Cyclic voltammograms of (a) (PCB)MnClCoCl, (b) (PCX)-MnClCoCl, (c) (PCO)MnClCoCl, (d) (Et_2Me_6PhPor)MnCl, and (e) (Me_4-Ph_5Cor)Co in pyridine, 0.1 M TBAP.

is assigned to the bis-pyridine adduct of the cobalt(III) corrole in the dyad. Similar spectral features are seen for (PCA)MnClCoCl (Table 1).

The UV−visible spectrum of the initial (PCB)MnClCoCl complex (Figure 10c) differs from that of the other manganese porphyrin dyads in pyridine in that it exhibits a relatively stronger porphyrin Soret band at 368 nm and a weaker visible band at 478 nm. It has the same 555−560 nm band as the other (PCY)MnClCoCl (Y = O, A, and X) dyads, but no 600 nm band is seen (Table 1).

The spectrum of singly reduced (Et_2Me_6PhPor)MnCl in pyridine exhibits an intense Soret band at 430 nm and a visible band at 555 nm, as shown by the dashed line in Figure 4a. This spectrum is typical of a manganese(II) porphyrin with one bound pyridine axial ligand,[39−41] i.e., (Et_2Me_6PhPor)Mn^{II}(py). The one-electron-reduction products of (PCO)MnClCoCl, (PCA)MnClCoCl, and (PCX)MnClCoCl also display an intense Soret at 429−431 nm, and all three dyads also have a visible band at 555−557 nm, thus suggesting that the Mn^{II} centers are also five-coordinate, as in the case of (Et_2Me_6PhPor)Mn^{II}(py).

As seen in Figure 10 and Table 1, the molar absorptivity of the $Co^{III}(py)_2$ marker band in (PCO)MnClCoCl and (PCA)MnClCoCl is the same as that in the monomer ($\epsilon = 1.7 \times 10^4$) but decreased in intensity by ∼50% in (PCX)MnClCoCl. Reduction of the Mn^{III} center to give the

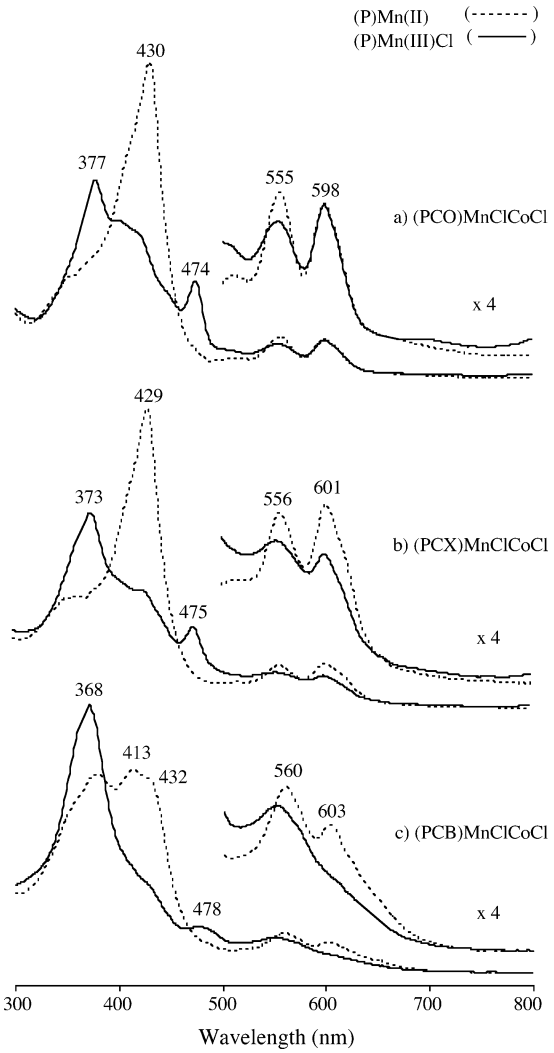

Figure 10. UV−visible spectra of (PCY)MnClCoCl (solid line) and the singly reduced species (dashed line) in pyridine, 0.1 M TBAP, where Y = O (a), X (b), and B (c).

manganese(II) porphyrin dyads is accompanied by no change in molar absorptivity for the $Co^{III}(py)_2$ band of PCO and PCA but a significant increase is seen for PCX, although the value is still less than those in the other dyads. This indicates that the cobalt(III) corrole is bis-ligated in the PCA and PCO dyads but exists as a mixture of five- and six-coordinate cobalt(III) pyridine complexes in the PCX derivative. Under these conditions, the mechanism for reduction is as shown in Scheme 4.

Again, the PCB dyad differs from those of the other dyads in terms of the UV−visible spectrum for the singly reduced compounds. Three relatively weak Soret bands are seen for Mn^{III} at 379, 413, and 432 nm. There is no 600 nm band in the spectrum of the initial complex, but it is seen for the singly reduced species (dashed line in Figure 10c), thus indicating that two pyridine molecules are bound to the cobalt corrole center in the singly reduced product on the UV−visible spectroelectrochemical time scale.

This similarity in Co^{III}/Co^{II} half-wave potentials for $(PCB)H_2Co$ and (PCB)MnClCoCl implies the same $Co^{III}(py)/Co^{II}$ process on the cyclic voltammetry time scale, but the presence of a 603 nm marker band for $Co^{III}(py)_2$ after the complete reduction of Mn^{III} to Mn^{II} by thin-layer spectroelectrochemistry (see Table 1) is consistent with a slow conversion of $Co^{III}(py)$ to $Co^{III}(py)_2$, as shown by the equilibrium in the lower part of Scheme 4.

Summary. Combined electrochemical and UV−visible spectoelectrochemical methods were utilized to elucidate the prevailing mechanisms for electroreduction of three different series of porphyrin−corrole dyads having the form $(PCY)H_2Co$ and (PCY)MClCoCl, where M = Fe^{III} or Mn^{III}. The compounds are all reduced in multiple stepwise one-electron transfers, the first of which involves the M^{III}/M^{II} process of the porphyrin or corrole in pyridine and is accompanied by the gain or loss of pyridine axial ligands depending upon the particular spacer in the dyad.

One aim of this study was to investigate how changes in the porphyrin unit of (PCY)MClCoCl and $(PCY)H_2Co$ would effect the binding of pyridine to the cobalt(III) corrole within the cavity, and this was easily accomplished by monitoring the reversibility or irreversibility of the Co^{III}/Co^{II} process by cyclic voltammetry while also following the reaction by thin-layer spectroelectrochemistry to ascertain the presence or absence of a 600 nm marker band assigned to $Co^{III}(py)_2$. The mono-pyridine cobalt(III) corroles all display reversible to quasi-reversible reductions at potentials close to −0.60 V vs SCE by cyclic voltammetry, while the bis-pyridine adducts are irreversibly reduced at potentials more negative than −1.10 V for a scan rate of 0.1 V/s. Thus, a combination of data from routine cyclic voltammetry at a scan rate of 0.1−1.0 V/s and the much slower thin-layer spectroelectrochemistry at 5−20 mV/s (or slower) provide more definitive information than that from just one of the two techniques alone while also giving some indication as to axial ligation kinetics because the two measurement techniques operate on different time scales of observing the electrogenerated reduction products.

A summary example of this is shown in Figure 11 for the case of the three PCB complexes. As earlier discussed, $(PCB)H_2Co$ is quasi-reversibly reduced at −0.59 V and displays no 600 nm marker band for the reduced product in the UV−visible spectrum. The electrochemical and spectroelectrochemical data are thus self-consistent and definitively indicate the dyad in solution to be $(PCB)H_2Co(py)$, which is also the assignment resulting from other experiments described in this paper and from a previously published structural characterization.[29]

A reversible Co^{III}/Co^{II} reaction is also seen for (PCB)MnClCoCl at −0.62 V, which leads to the assignment of $[(PCB)Mn^{III}(py)_2Co(py)]^+$ as the species in pyridine solutions when also considering the lack of a $Co^{III}(py)_2$ marker band and the known ligation properties of manganese(III) porphyrins. However, as seen in Figures 5, 10, and 11b, the reduction of $Mn^{III}(py)_2$ to $Mn^{II}(py)$ is accompanied on the slower spectroelectrochemical time scale by the appearance of a 603 nm band in the UV−visible spectrum. This is consistent with the addition of a second pyridine ligand to $Co^{III}(py)$ as one ligand is lost from the electrogenerated manganese(II) porphyrin, thus maintaining one pyridine

Scheme 4. Electroreduction Mechanisms for Dyads with Manganese(III) Porphyrins

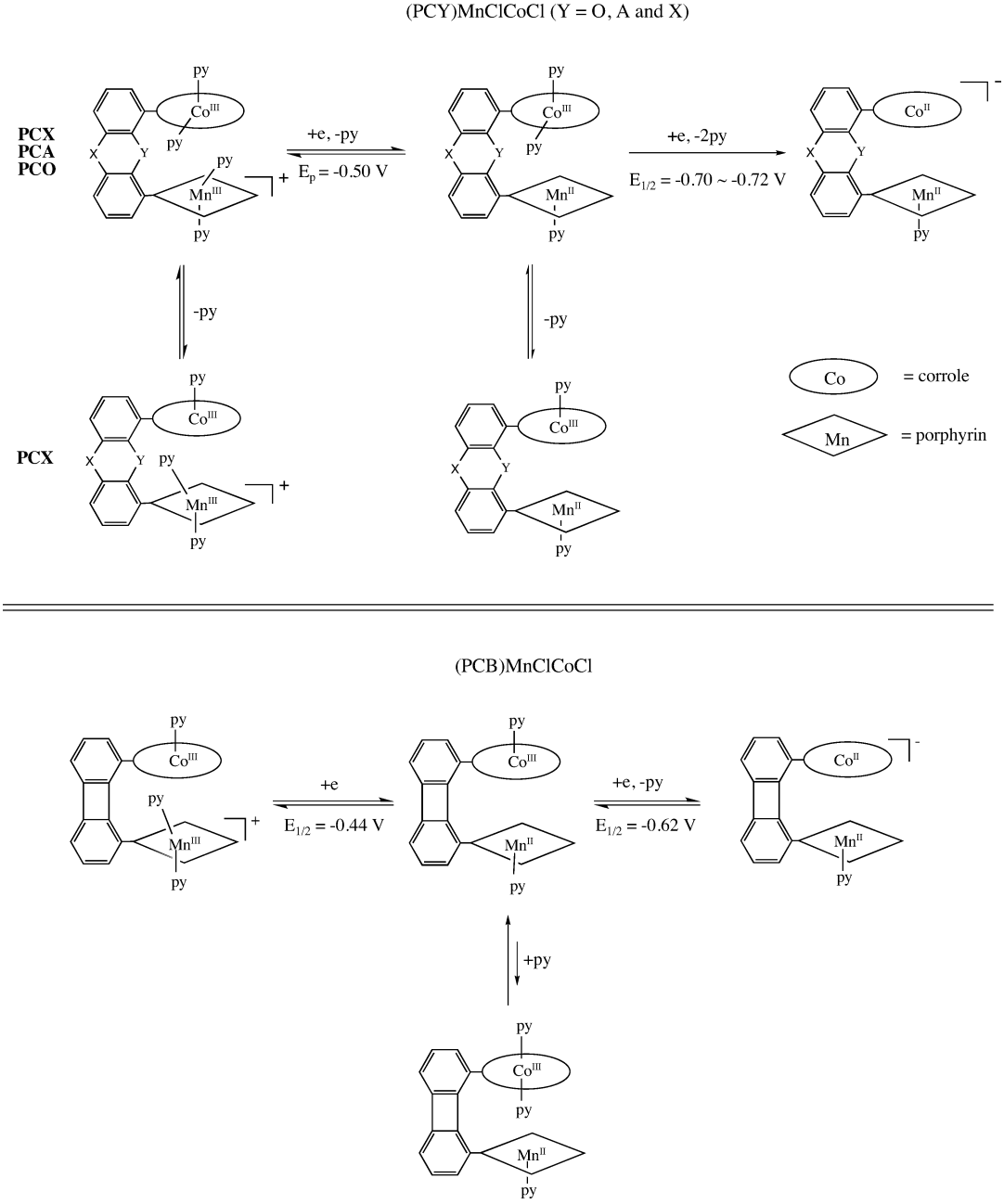

ligand within the cavity (for about 50% of the compounds, as determined by the reduced value of $Co^{III}(py)_2$ in Table 1).

A similar change in the corrole coordination number with a change in the the porphyrin metal oxidation state is also observed in the case of (PCB)FeClCoCl. Here the initial Fe^{III} complex can be assigned as (PCB)FeClCo(py) by virtue of its irreversible $Fe^{III}Cl/Fe^{II}$ reduction at −0.54 V (see the earlier discussion) and its lack of a bis-pyridine cobalt(III) marker band in the UV−visible spectrum. However, unlike $[(PCB)Mn^{III}(py)_2Co(py)]^+$, the addition of a second pyridine ligand to the corrole unit of $(PCB)Fe^{III}ClCo(py)$ is rapid after reduction of the porphyrin metal center, and this is indicated by the lack of a reversible Co^{III}/Co^{II} process in the cyclic voltammogram and the appearance of a fully formed 603 nm marker band, as seen in Figures 5, 6a, and 11c. Under these conditions, the Fe^{III} form of the dyad is coordinated by one pyridine ligand, while the Fe^{II} form has four bound pyridine axial ligands, with the overall reduction sequence proceeding as shown in eq 3.

Before starting this study, it was expected that porphyrin−corrole dyads with the largest spacers, namely, O and A, would readily accommodate the formation of cobalt(III) bis-pyridine adducts because of the larger size of the cavity, while dyads with the smallest B spacer would seem to have insufficient room to add even a single pyridine within the cavity, as was structurally seen in the case of $(PCB)H_2Co(py)$.[29]

The X linker has a size closer to that of B than to that of the O or A bridge, but because $(PCX)H_2Co(py)_2$ was characterized in the solid state,[42] either mono- or bis-pyridine adducts were thought to be possible for this dyad in solution.

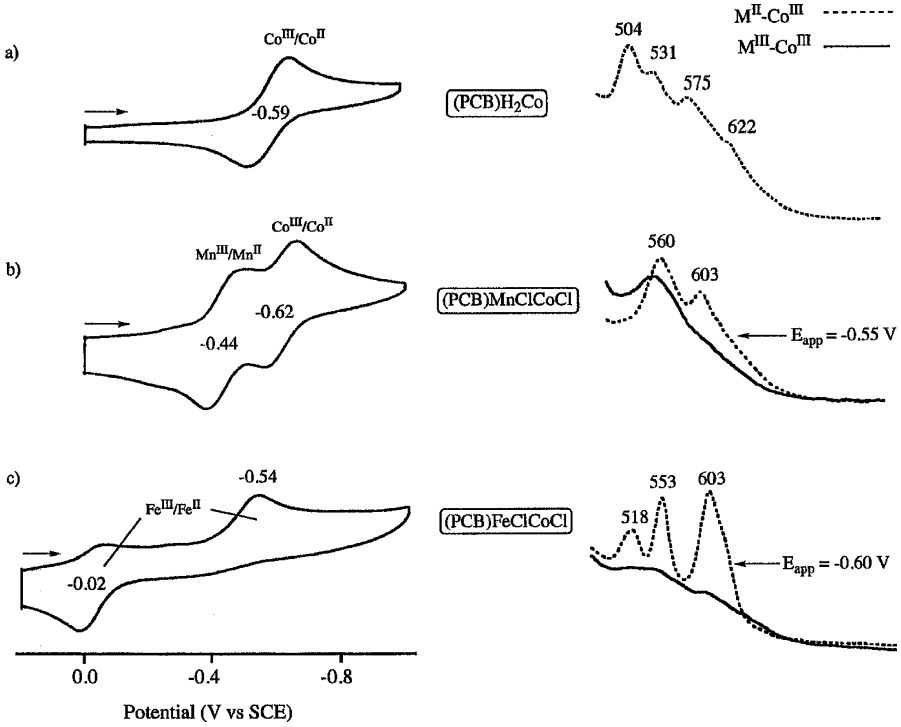

Figure 11. Cyclic voltammograms and visible bands of (a) (PCB)H_2Co, (b) (PCB)MnClCoCl, and (c) (PCB)FeClCoCl in pyridine, 0.1 M TBAP. Potentials for the formation of Mn^{II}/Co^{III} and Fe^{II}/Co^{III} are set at −0.55 and −0.60 V, respectively.

Table 5. UV−Visible Spectral Marker Band [λ_{max}, nm ($\epsilon \times 10^{-4}$ L mol^{-1} cm^{-1})] of the $Co^{III}(py)_2$ Unit of (PCY)MClCoCl Derivatives in Pyridine Containing 0.1 M TBAP

	porphyrin metal ion				
macrocycle	2H	Fe^{III}	Fe^{II} [b]	Mn^{III}	Mn^{II} [b]
PCO	599 (2.7)[a]	599 (1.5)	599 (1.5)	598 (1.7)	598 (1.7)
PCA	602 (2.7)[a]	600 (1.6)	600 (1.6)	600 (1.7)	600 (1.7)
PCX	602 (2.7)[a]	600 (1.5)	600 (1.6)	599 (0.9)	600 (1.4)
PCB	none	none	603 (1.7)	none	603 (0.8)

[a] A visible band of free-base porphyrin at 620−630 nm is overlapped by this band. [b] Electrogenerated in a thin-layer spectroelectrochemical cell.

This is indeed the case as shown in Table 5, which summarizes spectroscopic data on the 600 nm marker band for 20 different dyads containing five different porphyrins, eight of which were electrogenerated in solution.

This bis-pyridine marker band has a molar absorptivity of 1.7×10^4 for $(Me_4Ph_5Cor)Co^{III}(py)_2$ in pyridine (Table 1), and a similar value is seen for many of the investigated PCY derivatives in Table 4. The spectroscopic data confirm a $Co^{III}(py)_2$ assignment in all of the PCA and PCO derivatives, independent of the nature of the porphyrin center, be it 2H, Fe^{III}, Fe^{II}, Mn^{III}, or Mn^{II}. The 2H, Fe^{III}, and Fe^{II} complexes of PCX also exist as a bis-pyridine adduct in neat pyridine, but the decreased intensity of this band in the case of the Mn^{III} and Mn^{II} complexes is consistent with incomplete formation of the bis-adduct and the presence of an equilibrium involving $Co^{III}(py)_2$ and $Co^{III}(py)$. This is also seen in the electrochemical data that follow the overall reduction sequence of steps shown in Scheme 4.

Most surprising is what occurs in the case of the (PCB)FeClCoCl dyad, where the iron(III) porphyrin form of the complex is assigned as $(PCB)Fe^{III}ClCo^{III}(py)$ on the basis of combined electrochemical and spectroscopic data and the singly reduced form as $(PCB)Fe^{II}(py)_2Co^{III}(py)_2$. The measured molar absorptivity of the diagnostic 603 nm band is 1.7×10^4 (Table 4), exactly the same as that for the monomeric corrole, $(Me_4Ph_5Cor)Co^{III}(py)_2$, under the same solution conditions. Four pyridine molecules (with two inside the cavity) are also bound to the other PCY dyads with iron(II) and cobalt(III) corroles, and the overall electroreduction mechanism is as shown in Scheme 3.

The data in this study should prove valuable in designing porphyrin−corrole dyads with other linking bridges and should also be applicable to bis-corrole and bis-porphyrin systems, which are now being investigated as to their reactivity with CO, O_2, or other small molecules that may need to be bound to two metal centers within a cavity of two macrocycles in order to undergo a desired specific reactivity.

Acknowledgment. The support of the Robert A. Welch Foundation (Grant E-680 to K.M.K.) and the French Ministry of Research (MENRT), CNRS (UMR 5633), is gratefully acknowledged. The Region Bourgogne is acknowledged for a scholarship (F.B.), and the authors are also grateful to M. Soustelle for the synthesis of pyrrole and dipyrromethane precursors.

(42) Barbe, J.-M.; Burdet, F.; Espinosa, E.; Guilard, R. *Eur. J. Inorg. Chem.* **2005**, 1032−1041.

IC051073S